THE GEOLOGICAL SOCIETY OF AMERICA®

Sedimentary characteristics and origin of lacustrine organic-rich shales in the salinized Eocene Dongying Depression

Chao Liang[1,2,†], Zaixing Jiang[3], Yingchang Cao[1], Jing Wu[4], Yongshi Wang[5], and Fang Hao[1,2]

[1]*School of Geosciences, China University of Petroleum, Qingdao 266000, China*

[2]*Laboratory for Marine Mineral Resources, Qingdao National Laboratory for Marine Science and Technology, Qingdao 266071, China*

[3]*School of Energy Resources, China University of Geosciences, Beijing 100083, China*

[4]*Exploration and Production Research Institute, SINOPEC, Beijing 100083, China*

[5]*Geological Scientific Research Institute, Sinopec Shengli Oilfield, Dongying 257015, China*

ABSTRACT

Lacustrine organic-rich shales are well developed within the Eocene Dongying Depression in the Bohai Bay Basin in eastern China and across Southeast Asia. Understanding the sedimentation of these shales is essential to the study of depositional processes, paleoenvironment, and paleoclimate reconstruction. This study investigates the sedimentary characteristics and formation mechanisms of lacustrine shales in the upper fourth member of the Eocene Shahejie Formation (Es4s) within the Dongying Depression based on thin sections and field emission scanning electron microscope (FESEM) observations of well cores combined with X-ray diffraction and geochemical indicators. Six lithofacies were identified: (1) laminated calcareous mudstone, (2) laminated dolomitic mudstone, (3) laminated clay mudstone, (4) laminated gypsum mudstone, (5) massive mudstone, and (6) siltstone. The organic matter in the Es4s shale is mainly type I and type II kerogens, as well as a small proportion of type III kerogen. On the basis of lithofacies associations, paleosalinity values, redox properties, and terrigenous inputs, the lower Es4s shale can be divided into six intervals from bottom to top, numbered I, II, III, IV, V, and VI. The thickness of each interval ranges from several meters to more than 10 m, reflecting high-frequency oscillations in the environment of the lake basin, markedly different from a relatively stable marine environment.

The laminated mudstones are characterized by fine grain sizes, scarce large terrigenous debris (quartz and feldspar), and compositions that are rich in pyrite and sapropelic organic matter. These features indicate that these lithofacies were deposited out of suspension in a quiet water body characterized by a relatively low rate of deposition. The characteristic laminae of these lithofacies indicate subtle differences in depositional processes. The laminated gypsum mudstone was likely deposited in an evaporative environment, because its formation would have consumed Ca^{2+} and SO_4^{2-}, promoting the deposition of a laminated dolomitic mudstone. In contrast, laminated clay mudstone was deposited in a manner that increased the volume of small terrigenous materials. Deposition of this lithofacies was controlled by the nature of the water body, paleoclimate, and terrigenous inputs. Laminated mudstones are dominant in the lower Es4s shale, suggesting that suspension was the main depositional process leading to formation of the lower Es4s shale. In contrast, the massive mudstones were likely rapidly deposited associated with siltstone as the result of fine-grained turbidites. The lower Es4s shale was formed in a depositional environment composed of a saline, medium-depth lake under anoxic conditions, with limited terrigenous inputs. The depositional process included suspension and turbidity currents. The high salinity is suggested to be related to a marine transgression, which may have been facilitated by a rise in sea level caused by global warming in the early Eocene, together with the large-scale tectonic activity of East Asia. Seawater input affected the lithofacies, influenced lake water body conditions, triggered turbidity currents, and prompted the accumulation of organic matter. The deposition of the Es4s shale in the Dongying Depression may help us to understand the deposition of lacustrine shale, paleoclimate reconstructions for the Eocene, and the tectonic activity of East Asia.

INTRODUCTION

Fine-grained sedimentary rocks mostly contain grains that are smaller than 62.5 μm and comprise approximately two thirds of the stratigraphic record (Aplin et al., 1999; Stow and Mayall, 2000; Tucker, 2001; Aplin and Macquaker, 2011). Of these rocks, mudstones consist of a variable mixture of clay minerals, quartz, feldspars, carbonates, sulfides, amorphous material, and organic matter (Macquaker and Adams, 2003; Potter et al., 2005; Milliken, 2014). Organic-rich mudstones, in particular, act as important petroleum sources, reservoirs for shale oil and gas, and seals in conventional reservoirs (Schieber, 1999; Andersson and Worden, 2004; Bowker, 2007; Jarvie et al., 2007; Abouelresh and Slatt, 2012). Because of its apparent homogeneity and the limitations of ultramicroscopic experimental equipment, shale has been often overlooked in sedimentological studies over recent decades (Arthur and Sageman, 1994; Schieber, 1999; Potter et al., 2005; Jiang et al., 2013). However, because of extensive and successful deep-water hydrocarbon exploration, especially for shale oil and gas (Hill et al., 2007; Loucks and Ruppel, 2007; Slatt, 2007; Kuang et al., 2012), deep-water sedimentation has become the focus of considerable attention, including the depositional environments, transport, and depositional processes associated with organic matter preservation in black shales (Macaquaker et al., 2007, 2010b; Piper and Calvert, 2009; Aplin and Macquaker, 2011; Konitzer et al., 2014; Liang et al., 2016).

The depositional processes leading to black shales mostly involve pelagic and hemipelagic settings, turbidity currents, debris flows, slides, and wave-enhanced sediment gravity flows (Stow and Bowen, 1980; Stow and Mayall, 2000; Soyinka and Slatt, 2008; Bouma and Stone, 2000; Macquaker et al., 2010a; Ghadeer

†liangchao0318@163.com

GSA Bulletin; January/February 2018; v. 130; no. 1/2; p. 154–174; https://doi.org/10.1130/B31584.1; 16 figures; 3 tables; published online 29 August 2017.

and Macquaker, 2011; Ochoa et al., 2013; Plint, 2014). One or more of these processes may contribute to the deposition of a black shale, suggesting that mud may not always be the product of "low-energy" or "quiet-water" deposition (Cheel, 1990; Konitzer et al., 2014; Frébourg et al., 2016). Indeed, flocculation processes contribute to the long-distance transport of large amounts of muddy marine sediments (Schieber et al., 2007; Macquaker et al., 2010a; Aplin and Macquaker, 2011), and flume experiments have shown that flocs can be present as a hydraulic equivalent in coarse clastics, transported by high-density flows and turbidity currents on the seabed (Schieber and Southard, 2009; Schieber et al., 2010). Most studies to date, however, have focused on marine shales, and many of these are siliciclastic. In contrast, research on lacustrine organic-rich shales has been rarely reported, particularly carbonate-rich examples (Burton et al., 2014; Liu et al., 2015; Roop et al., 2015). While the deposition of marine siliciclastic shale mainly results from physical and chemical processes, carbonate-rich shales are instead predominantly biochemical in origin (Schieber et al., 2007; Macquaker et al., 2010b; Aplin and Macquaker, 2011; Jiang, 2011). Such lacustrine carbonate-rich shales are widely developed in Mesozoic and Cenozoic terrestrial strata across Southeast Asia (Butterworth and Wain, 1995; Tänavsuu-Milkeviciene and Sarg, 2012; Xu et al., 2014), but obvious differences between them and marine siliciclastic shales include the structural backgrounds of the basins, material compositions and sources, sedimentary environments, and depositional processes (Jiang et al., 2013; Burton et al., 2014).

Recently, due to increasing demand for unconventional oil and gas exploration, especially shale oil and gas in China (Song et al., 2013; Wang et al., 2013; Zou et al., 2013), the Sinopec Shengli Oilfield company initiated research aimed at the exploration of lacustrine shale oil in the Dongying Depression of the Bohai Bay Basin. The study intervals targeted in this research were 200 m sequences within the Paleogene lower Es4s black shale, which is predominantly composed of carbonate and clay minerals. The sedimentary characteristics and mechanisms of formation of the black shale are discussed in detail in this paper. Here, we characterize the lithofacies of lacustrine carbonate-rich black shales within the Es4s unit, analyze the depositional environments and processes, and discuss the salinization of lake water and accumulation of organic matter. This study will help in understanding lacustrine shale deposition and comparisons with marine shale, paleoclimate reconstructions, tectonic activity, and depositional responses in Eocene East Asia.

GEOLOGICAL SETTING

Bohai Bay Basin, a fault depression basin developed in the Paleozoic North China craton basement (Fig. 1A), is located in eastern China and is filled by Mesozoic–Cenozoic strata. The formation of the Bohai Bay Basin was controlled by the evolution of the tectonic framework in East Asia. During the later Cretaceous–Paleocene, the Indian plate and the Pacific plate subducted under the Eurasian plate, from south to north, and from east to west, respectively (Li et al., 2013; Ding et al., 2014). At ca. 55 Ma, the rate of Pacific plate movement decreased and resulted in strong retreating extension in the eastern part of East Asia, forming a series of sedimentary basins (Zhang et al., 2014; Zhao and Li, 2016). Bohai Bay Basin was formed under this framework, during which a series of half-graben lake basins formed, including the Dongying Depression.

The Dongying Depression is located in the southeastern Bohai Bay Basin (Fig. 1B). This depression is 5700 km^2 in total area, bordered by the Luxi and Guangrao uplifts to the south, the Chenjiazhuang uplift to the north, the Linfanjia and Gaoqing uplifts to the west, the Qingtuozi uplift to the northeast, and the Wangjiagang fault belt to the southeast. The Dongying Depression includes four sags, the Lijin, Boxing, Niuzhuang, and Minfeng (Fig. 1C).

The Dongying Depression is a typical half-graben lake basin, with a steep slope in the north and west controlled by faults and a gentle slope in the south and east. The Chennan fault in the north and the Pingnan fault and Gaoqing fault in the west are the main boundary faults, which control the lake basin evolution. The tectonic evolution of the Dongying Depression included two stages, rifting (65–24.6 Ma) and postrifting thermal subsidence (24.6 Ma–; Liu et al., 2004; Li et al., 2007; Lin et al., 2009; Yang et al., 2009; Lu et al., 2013). According to the subsidence rate, the first stage can be further divided into four periods (i.e., rifting I, II, III, and IV): initial period (I), development period (II), peak period (III), and atrophy period (IV), corresponding to members of the Eocene Kongdian Formation (Ek) and Shahejie Formation (Es), Ek, Es4, Es3-Es2x, and Es2s-Ed, with the study interval (Es4s) falling within rifting period II (Fig. 2). In the initial rifting period (rifting I), fault activity was weak, and the basin subsidence rate was low, and so shallow-water facies deposits developed, including braided fluvial facies. After initial rifting occurred in the Kongdian period, accompanying intensive fault activity, the Dongying Depression entered into a strong rifting stage in rifting period II (Es4). During the rifting II period, the lake basin subsided quickly with a large-scale lake expansion. In this stage, a large area of semideep lake facies developed (Ren and Zhang, 2004; Guo et al., 2010; Jiang et al., 2011).

The study area is composed of Cenozoic basin-filling strata with local thicknesses up to 5000 m in the depocenter, including the Kongdian (Ek), Shahejie (Es), Dongying (Ed), Guantao (Ng), Minghuazhen (Nm), and Pingyuan (Qp) Formations. Of these, the Shahejie Formation can be further subdivided into four members from top to bottom, Es1, Es2, Es3, and Es4. Although this basin started to expand after the Mesozoic, reaching a maximum in the period during deposition of Es4s and Es3x (i.e., rifting II and III; Qiu et al., 2006; Sheng et al., 2008; Xue et al., 2013), during the latter period, the Dongying Depression mainly was a semiclosed saline lake environment with anoxic conditions formed at the lake bottom (Liu et al., 2001; Zhu and Jin, 2003), which prevented the oxidation of organic matter. At the same time, the warm and humid paleoclimate of this period promoted bioactivity and provided abundant paleoproductivity (Zhu et al., 2005; Wang et al., 2012). Thus, the Es4s member mainly comprises an ~200-m-thick organic-rich "black shale," which is our study interval.

METHODS

The basic data presented here include a 312 m section of core from two wells (NY1 and LY1; Fig. 1C), as well as 216 thin sections, 48 field emission scanning electron microscope (FESEM) samples, and analyses of rock pyrolysis, maceral composition, and organic carbon data from 48 samples, X-ray diffraction data from 192 well NY1 samples that were collected at ~0.25 m intervals, and geochemical element analysis of 45 samples from well NY1 that were collected at ~1.25 m intervals. Mineral X-ray diffraction was performed using a D/max-2500 TTR in Shengli Oilfield, Sinopec, Dongying City, Shangdong province, China; prior to analysis, each sample was oven-dried at 40 °C for 2 d and ground to <40 mm using an agate mortar to thoroughly disperse minerals. Subsequent computer diffractogram analysis enabled identification and semiquantitative investigation of the relative abundances (wt%) of the various mineral phases, while total organic carbon (TOC) was determined using a LECO carbon-sulfur analyzer CS600 in Shengli Oilfield, Sinopec, Dongying City, Shandong province, China at a test temperature of 27 °C. The measurement technique used here was based on sample combustion in an O_2 atmosphere to convert TOC to CO_2. Ar ion-beam milling was used to prepare samples for nanopore imaging, and

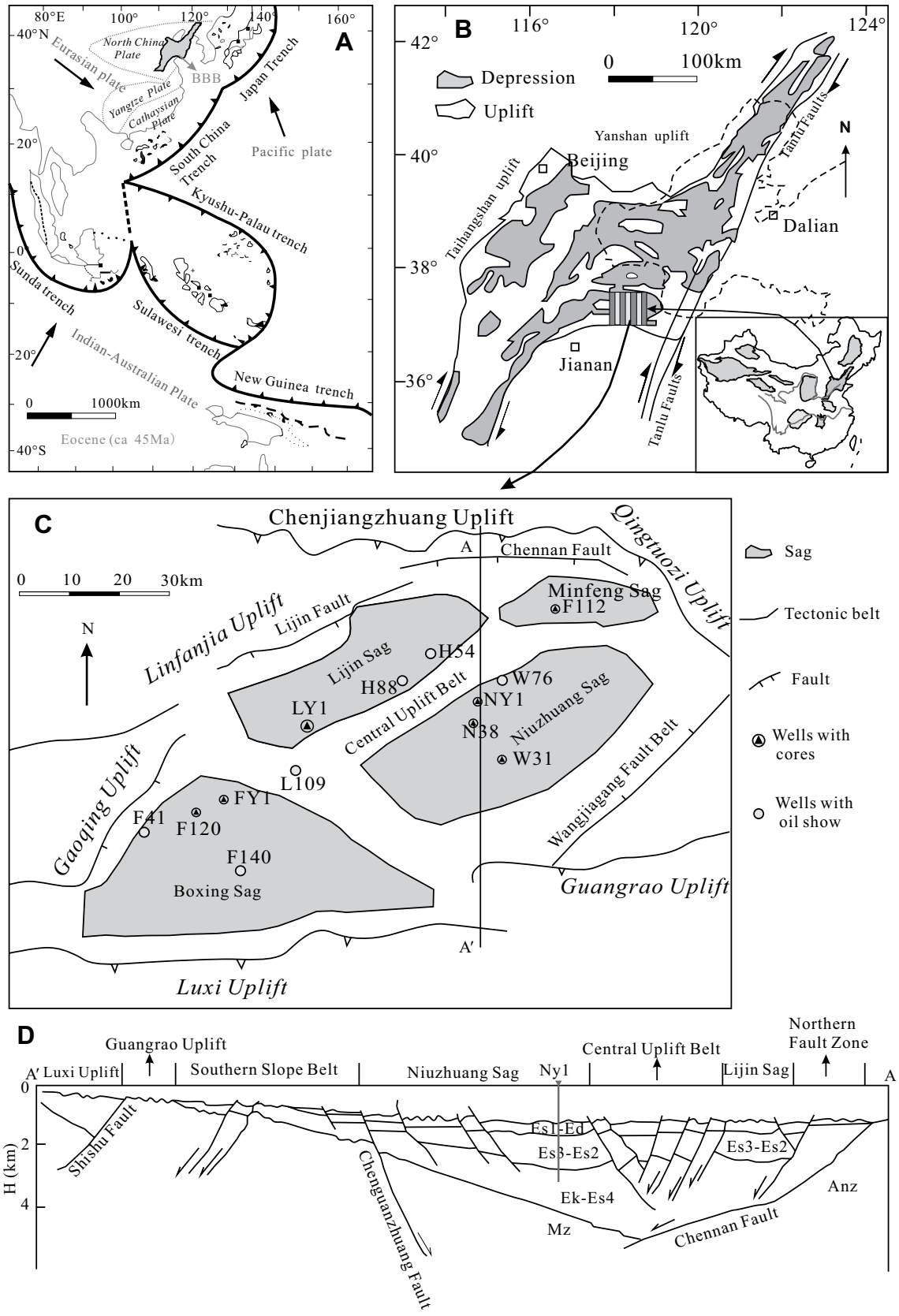

Figure 1. Regional map of the study area. (A) Tectonic framework of the East Asia in the Eocene. (B) Structural map of Bohai Bay Basin (BBB) and the location of Dongying Depression (box). (C) Structural map showing key well locations. (D) Structural cross section (for the location, see part B).

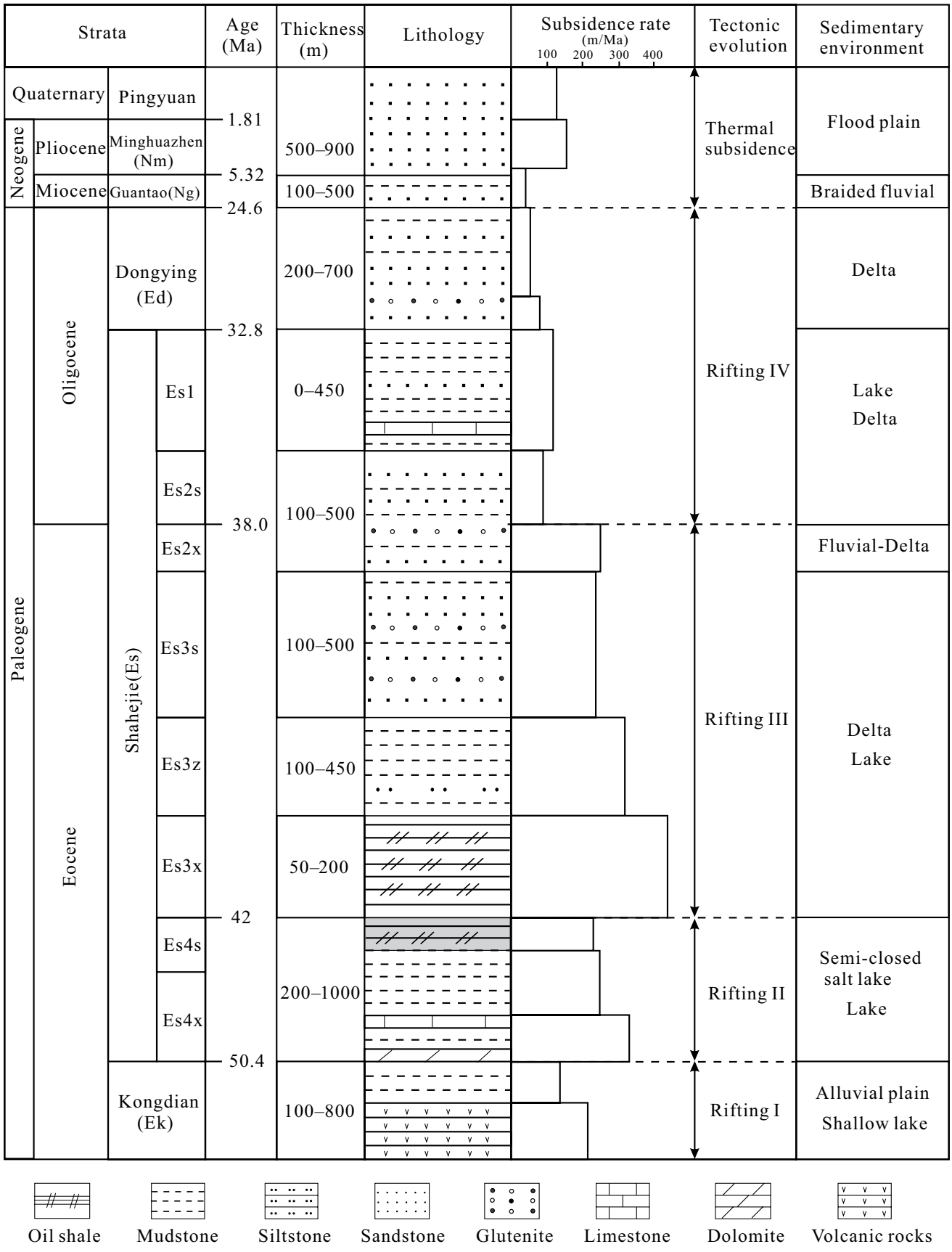

Figure 2. Sedimentary facies and stratigraphic column of the Dongying Depression.

high-resolution FESEM was used to observe micro- and nanosize pores. All samples were coated in gold and observed using a Hitachi S-4800 (FESEM equipment, Beijing Normal University, Beijing, China) with the working current set to 10 kV. The lithology and mineralogy of target layer intervals in the study area were based on detailed observations of cores, thin sections, scanning electron microscope (SEM) observations, and whole-rock and clay mineral X-ray diffraction analyses. Source rock characteristics were described in terms of their organic maceral compositions, TOC tests, and backscattered SEM analyses, while geochemical elements were used to analyze sedimentary environments. In this context, Sr/Ba and B/Ga ratios and biomarkers were used as proxies for paleosalinity, Th/U and Ni/Co ratios were used as proxies for anoxic conditions, and Co, Cr, K, Ni, Al, Ti, and Na values and the Fe/Mn ratio were used as proxies for sediment provenance. A depositional model was established by integrating lithofacies, organic geochemistry, and element analyses.

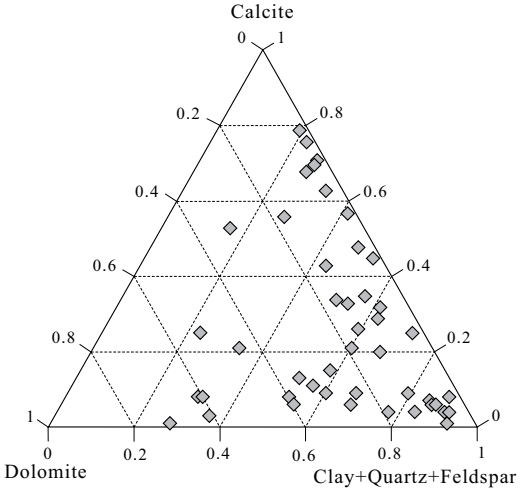

Figure 3. Ternary plot to show the whole-rock mineral composition of the Es4s shale in the study area. Note that because of its limited distribution (only at the base of the Es4s shale) and small number of samples, anhydrite data were not collected or used in this figure.

RESULTS

Lithofacies and Petrology

Mineralogy

The Es4s shale is composed of carbonate, clay minerals, quartz, subordinate plagioclase (Fig. 3), K-feldspar, pyrite, and anhydrite (Table 1). Of these, carbonates are the dominant minerals (average: 43.67 wt%), and the dolomite content (average: 19.48 wt%) is inversely proportional to the calcite content (average: 24.19 wt%). Calcite in the Es4s shale is mainly present in clay- to silt-sized crystalline form and contains small amounts of calcareous biological debris, for example, ostracod fragments, while dolomite mainly occurs in clay-sized crystalline form, either as dolomite laminae or pellets (Fig. 4A), and quartz is also common (average: 17.5 wt%). Quartz are mainly clay- to silt-sized minerals in two forms, clastic particles within the massive and laminated silty shale that have particle sizes greater than 10 μm, and microcrystalline quartz that is much less than 10 μm in particle size and is surrounded by clay minerals (Fig. 4B). These clay minerals are by far the most abundant in the lower Es4s shale (average: 21.2 wt%); they are mainly illite and illite/smectite mixed layers (Fig. 4C), while feldspar content ranges between 2 wt% and 17 wt% (average: 7.68 wt%), and pyrite content ranges between 1 wt% and 12 wt% (average: 3.81 wt%), mainly occurring as framboids in the range between 5 μm to 20 μm, surrounded by clay minerals (Fig. 4D). Anhydrite minerals are common at the base of the Es4s shale (Fig. 4E), ranging in content between 1 wt% and 40 wt%.

Our results show that the mineral composition of the lower Es4s shale varies considerably and frequently in a vertical direction (Fig. 5). Clay and quartz contents are rich within two intervals, between 3492 m and 3888 m and between 3475 m and 3467 m, occurring at averages of 45.2 wt% and 26.1 wt%, respectively. In other intervals within the section, these minerals occur at much lower proportions, on average 18.6 wt% and 15.3 wt%, respectively. In addition, anhydrite is mostly abundant at the base of the Es4s shale and is scarce in other intervals (Fig. 5), while carbonate content is high throughout, with the exception of the two intervals noted above that are rich in clay and quartz. Calcite content is inversely proportional to dolomite content, while the latter is relatively high within the anhydrite-rich interval.

Lithofacies and Petrology

The laminated calcareous mudstone lithofacies is the predominant lithofacies within the Es4s shale. In hand specimens, the laminated calcareous mudstone is grayish black or dark gray, characterized by a high calcite content between 25 wt% and 79 wt% (average: 49.4 wt%) and rare clay minerals and terrigenous silts (Table 2). Laminae are well developed and horizontal or wavy (Figs. 6A–6C), while somewhat deformed laminae and lenticular bedding are also present (Figs. 6B and 6D). Cores and thin sections show clear laminar boundaries, comprising pure components (Fig. 6A); light laminae are mainly calcite with subordinate silts, while their darker counterparts are mainly clay and organic matter. Calcite laminae are mainly micritic, and fragments of ostracods are common (Fig. 7A); recrystallized calcite laminae can also be observed in cores and microscopic thin section, mainly occurring as "needles" or as closely packed crystal grains (Fig. 7B). This lithofacies is rich in type I organic matter, mainly planktonic algae (Fig. 8; Table 2), and I has a TOC content that ranges from 0.99 wt% to 4.22 wt% (average: 2.24 wt%).

The laminated dolomite mudstone lithofacies within the Es4s shale is typically a light-gray color in hand specimens (Figs. 6E and 6F) and has a dolomite content that ranges between 27 wt% and 70% (average: 44.2 wt%; Table 2). The dolomite in this laminated dolomitic mudstone mainly occurs as laminae within hidden crystals, microcrystals, or bright crystals (Figs. 7C and 7D), some of which are associated with rhombic automorphic crystals of anhydrite (Fig. 6F). This dolomite-enriched laminated dolomitic mudstone has a low TOC content (average: 1.6 wt%) and organic matter laminae that are thinner than their dolomitic counterparts (Fig. 7C). In addition, algal dolomite pellets can be seen in parts of these dolomite laminae (Figs. 7E and 7F), mixed with organic matter; these algal laminated dolomitic mudstones are rich in organic matter and have TOC contents up to 4.07 wt%.

In hand specimens, the laminated clay mudstone lithofacies within the Es4s shale is grayish black or completely black (Figs. 6G and 6H). Indeed, some samples of this lithofacies partly comprise thick homogeneous laminae with unclear boundaries(Fig. 6G), while others have well-developed thin laminae with clear boundaries (Fig. 6H). Both types consist of light organic-poor but quartz-rich clay laminae as well as laminae composed of dark organic-rich clay (Fig. 7G). This lithofacies has a high clay mineral content (average: 37.8 wt%) and an intermediate quartz content (average: 19.6 wt%), while the proportion of carbonate minerals is relatively low (Table 2). The laminated

TABLE 1. TOTAL ORGANIC CARBON (TOC) CONTENT (WT%), ROCK-EVAL PARAMETERS, AND MINERAL CONTENT (WT%) OF THE EOCENE SHALE IN DONGYING DEPRESSION

Depth (m)	TOC (wt%)	*S1* (mg/g)	*S2* (mg/g)	*T*max (°C)	*S1+S2* (mg/g)	*S1/S1+S2* (%)	*S1/TOC* (mg/g)	C (wt%)	Q (wt%)	F (wt%)	Cal (wt%)	Dol (wt%)	Py (wt%)	An (wt%)
3440.83	2.08	3.21	12.5	443	15.71	0.20	154	9	8	2	76	0	3	–
3441.87	4.29	5.34	25.02	445	30.36	0.18	124	35	20	9	20	13	3	–
3442.83	0.94	2.84	3.86	427	6.7	0.42	302	6	19	3	3	61	8	–
3443.83	1.82	3.19	9.27	443	12.46	0.26	175	11	11	3	71	2	2	–
3444.78	2.62	7.44	10.6	430	18.04	0.41	284	23	14	5	43	14	1	–
3445.78	2.77	4.85	11.01	431	15.86	0.31	175	35	22	9	6	27	2	–
3446.79	1.78	2.85	9.22	442	12.07	0.24	160	5	12	2	25	52	4	–
3447.73	2.74	9.62	13.75	433	23.37	0.41	351	22	18	7	8	40	5	–
3448.86	2.58	8.7	10.05	413	18.75	0.46	337	23	22	5	5	40	4	–
3450.02	3.42	6.68	15.29	439	21.97	0.30	195	17	18	15	33	14	3	–
3451.04	2.33	4.61	9.86	429	14.47	0.32	198	30	27	10	25	3	5	–
3452.04	1.83	3.79	7.96	433	11.75	0.32	207	6	13	5	68	6	2	–
3453.04	1.89	3.26	9.76	442	13.02	0.25	172	19	19	6	48	4	4	–
3453.99	1.13	4.23	4.39	425	8.62	0.49	374	3	8	2	53	31	3	–
3457.77	1.99	6.1	8.47	433	14.57	0.42	307	11	13	5	21	45	5	–
3458.64	4.07	7.01	16.73	439	23.74	0.30	172	13	11	6	8	60	2	–
3459.85	2.86	3.65	11.34	440	14.99	0.24	128	28	17	7	13	27	6	–
3461.01	1.61	8.35	7.06	424	15.41	0.54	519	8	11	6	56	17	2	–
3462.58	3.83	6.43	13.45	435	19.88	0.32	168	21	21	13	32	7	6	–
3463.59	3.64	19.07	21.52	432	40.59	0.47	524	25	19	5	13	35	3	–
3464.55	1.95	3.1	6.48	434	9.58	0.32	159	9	8	6	70	3	4	–
3465.69	1.74	4.13	5.85	418	9.98	0.41	237	30	18	8	21	19	4	–
3466.59	2	4.8	7.66	430	12.46	0.39	240	30	20	5	26	15	4	–
3467.61	0.69	0.56	0.7	428	1.26	0.44	81	50	26	9	8	3	4	–
3468.65	0.15	0.06	0.03	439	0.09	0.67	40	24	37	13	9	12	5	–
3471.44	0.39	0.82	0.82	425	1.64	0.50	210	50	25	6	5	4	4	–
3472.49	0.18	0.08	0.11	424	0.19	0.42	44	54	22	6	5	5	3	–
3473.45	0.27	0.23	0.35	421	0.58	0.40	85	50	26	10	3	5	5	–
3474.49	0.36	0.23	0.31	410	0.54	0.43	64	47	32	11	0	7	2	–
3475.49	1.06	1.09	2.76	437	3.85	0.28	103	5	12	2	0	57	12	–
3476.48	1.68	1.96	5.52	440	7.48	0.26	117	21	16	9	45	2	7	–
3477.28	1.23	1.86	2.67	418	4.53	0.41	151	53	23	11	4	4	4	–
3478.24	1.18	6.18	3.84	422	10.02	0.62	524	11	13	4	0	70	–	–
3480.23	3.07	9.22	11.91	435	21.13	0.44	300	30	19	9	9	31	2	–
3481.35	4.22	6.22	13.54	436	19.76	0.31	147	15	16	17	34	16	2	–
3482.28	2.17	4.27	6.29	416	10.56	0.40	197	11	33	6	35	9	6	–
3483.23	0.99	3.26	3.63	429	6.89	0.47	329	2	0	17	79	2	–	–
3484.58	2.75	9.58	9.24	422	18.82	0.51	348	29	20	10	27	9	3	–
3485.44	2.04	2.94	5.75	444	8.69	0.34	144	12	11	11	57	2	5	1
3486.44	1.5	4.44	4.61	431	9.05	0.49	296	18	14	5	8	30	3	22
3489.12	1.54	3.24	4.13	424	7.37	0.44	210	49	22	10	7	8	2	0
3490.04	0.87	3.79	1.59	425	5.38	0.70	436	44	24	9	4	13	4	0
3491.61	1.38	3.93	3.74	425	7.67	0.51	285	39	21	11	3	18	4	3
3492.7	2.08	3.85	5.4	415	9.25	0.42	185	12	9	4	2	29	3	40
3494.82	0.9	2.74	2.43	433	5.17	0.53	304	36	14	8	1	0	2	37
3495.75	2.48	3.09	6.02	439	9.11	0.34	125	7	10	15	63	2	1	2
3496.73	2.44	9.98	7.71	433	17.69	0.56	409	36	17	9	9	24	2	2
3497.97	0.44	0.53	0.72	426	1.25	0.42	120	10	9	3	0	38	2	37

Note: TOC—remnant total organic carbon, S1—free hydrocarbon, S2—pyrolyzed hydrocarbon, C—clay, Q—quartz, F—feldspar, Cal—calcite, Dol—dolomite, Py—pyrite, and An—anhydrite.

clay mudstone lithofacies also has a relatively high TOC content, ranging between 1.38 wt% and 4.29 wt% (average: 2.27 wt%); the organic matter in this lithofacies is mainly sapropelite-rich in dark laminae, mixed with difficult to distinguish clay minerals (Fig. 7G).

A laminated gypsum mudstone lithofacies is developed mainly toward the base of the Es4s shale. This lithofacies is shades of gray in color (Fig. 6I) and is characterized by a high anhydrite content (average: 34 wt%). Most of the other materials within the laminated gypsum mudstone consist of clay and dolomite (Table 2), and this lithofacies comprises a series of light anhydrite-rich and dark clay-rich laminae. Anhydrite occurs in serial laminae or "fragmented" forms, and examples of minerals with swallow-tail twins can be observed (Fig. 6I). Microscope images show that anhydrite is mainly present as euhedral crystals (Figs. 7H and 7I), usually occurring alongside dolomite (Fig. 7I). Overall, this laminated gypsum mudstone lithofacies has a low TOC content, on average just 0.84 wt% (Table 2).

A gray/blue-gray massive mudstone lithofacies is common in all the well cores within the Es4s shale (Fig. 6J), occasionally developed into indistinct horizontal bedding that clearly distinguishes it from the laminated mudstones. This massive mudstone shows mainly abrupt contacts with the overlying massive siltstone, as well as laminated shales to a lesser extent (Fig. 6K), and it is easily identified by its internal homogeneity and structure (Fig. 7J). The mineral composition of this massive mudstone lithofacies predominantly includes clay minerals (greater than 50 wt%), quartz (ranging between 10 wt% and 30 wt%), and a small amount of calcium. The silt grains within this unit are disorganized and do not indicate a particular flow direction, while pyrite aggregates are abundant. In addition, small volumes of ostracod debris and orientated carbon dust are also present (Fig. 7J); geochemical analysis shows that the TOC content of the massive mudstone is very low, on average 0.42 wt%, much lower than that of the laminated mudstones. Compared to the other lithofacies in the Es4s shale, this massive mudstone also has a significantly high vitrinite content (Fig. 8; Table 2).

A siltstone lithofacies is mainly developed within the lower Es4s shale and has single layer thicknesses ranging between 0.05 m and 0.5 m. The laminae that make up this sediment are

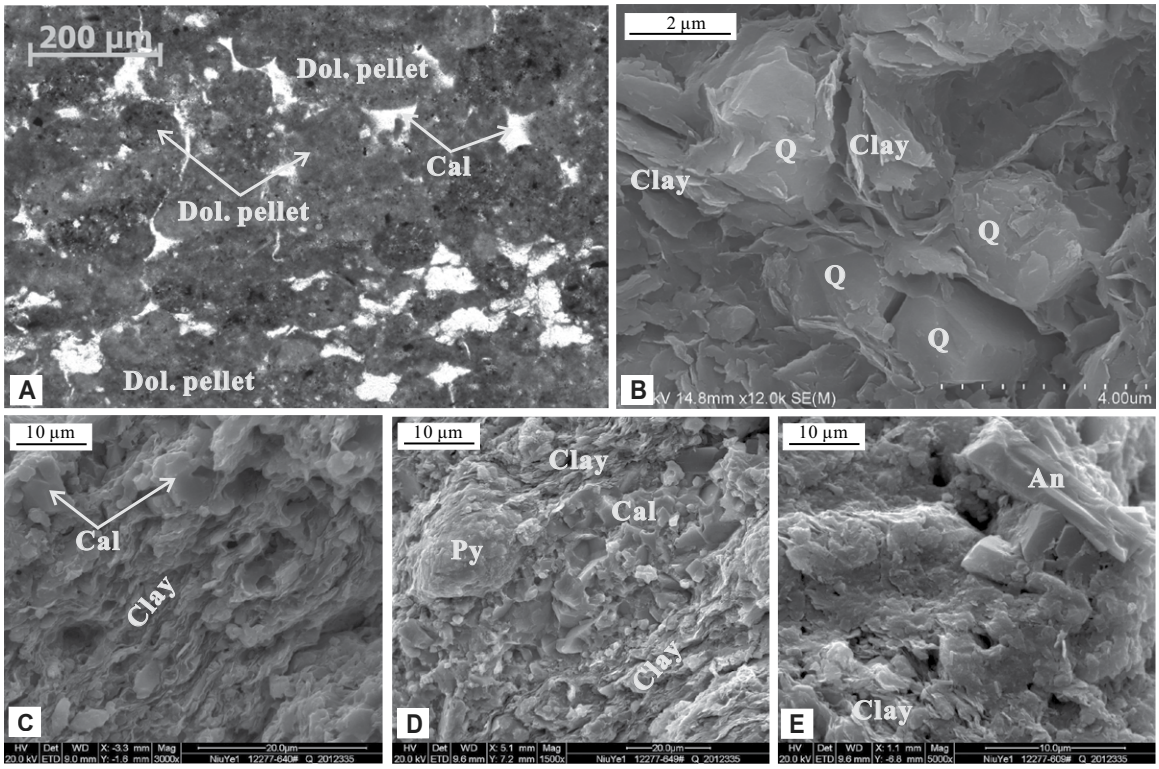

Figure 4. Mineral characteristics of the Es4s shale in well NY1 (depths in brackets). (A) Dolomite (Dol.) pellets with grain sizes between 50 μm and 200 μm that are cemented by the calcite (Cal; well NY1: 3485.96 m). (B) Microquartz (Q) surrounded by clay minerals of grain size 2 μm (well NY1: 3456.5 m). (C) Layered clay minerals (well NY1: 3459.2 m). (D) Framboidal pyrite (Py) surrounded by clay minerals and calcite (well NY1: 3462.58 m). (E) Anhydrite (An) in pores (well NY1: 3448.72 m).

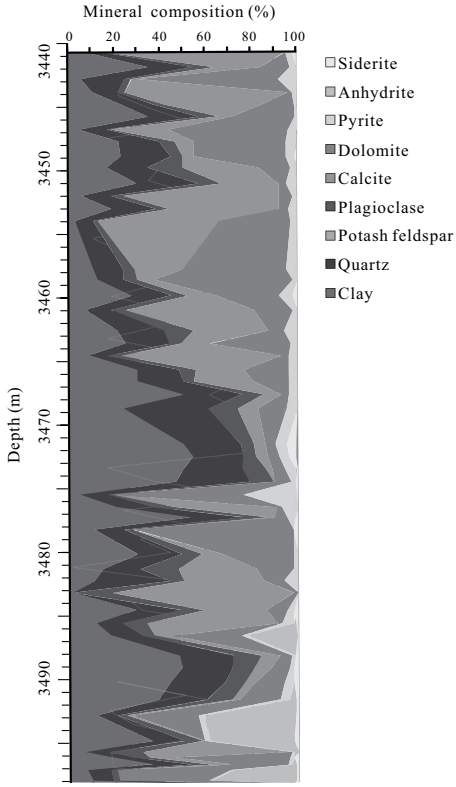

Figure 5. The mineral composition of the lower Es4s shale in well NY1.

greatly contorted and sometimes upright, while graded bedding can also be observed as the grain size changes from silt to mud (Fig. 6K). Rippled bedding and truncated structures are also developed within this lithofacies (Fig. 6L), which is associated with the blue-gray, organic-poor massive mudstone.

Organic Geochemical Characteristics

Organic Matter Types

Our maceral determinations of samples show that the Es4s shale predominantly contains sapropelinite and exinite. Additional Rock-Eval analysis demonstrates that the hydrogen index (HI) primarily ranges from 60 mg HC (hydrocarbons/g TOC to 987.1 mg HC/g TOC (average: 564.9 mg HC/g TOC), while the maximum yield temperature (Tmax) value ranges between 410 °C and 445 °C (average: 431 °C; Fig. 8; Table 1).

TABLE 2. AVERAGE VALUE OF MINERAL COMPOSITION OF DIFFERENT MUDSTONE LITHOFACIES

Lithofacies	TOC (wt%)	Calcite (wt%)	Dolomite (wt%)	Feldspar (wt%)	Quartz (wt%)	Clay (wt%)	Anhydrite (wt%)	Organic matter type
LCM-1 (18)	0.99–4.22 (2.25)	25–79 (49.5)	0–31 (8.3)	2–17 (8.6)	0–33 (14.95)	2–30 (14.9)	–	I
LDM (13)	0.94–4.07 (2.32)	0–25 (9.2)	27–70 (44.2)	2–9 (5.3)	11–22 (16.2)	5–35 (17.8)	–	I
LCM-2 (5)	1.38–4.29 (2.27)	3–21 (12)	8–24 (16.4)	8–11 (9.4)	17–22 (19.6)	30–49 (37.8)	–	I
MM (8)	0.15–0.69 (0.42)	0–9 (4.8)	3–13 (6.6)	6–13 (9.4)	22–37 (26.9)	24–54 (46.5)	–	III, I
LGM (4)	0.44–2.08 (0.84)	0–2 (1)	0–38 (22.3)	3–8 (5)	9–14 (10.7)	10–36 (19.3)	22–40 (34)	I

Note: Six lithofacies of the lower Es4s shale: (1) laminated calcareous mudstone (LCM-1), (2) laminated dolomitic mudstone (LDM), (3) laminated clay mudstone (LCM-2), (4) laminated gypsum mudstone (LGM), (5) massive mudstone (MM), and (6) siltstone.

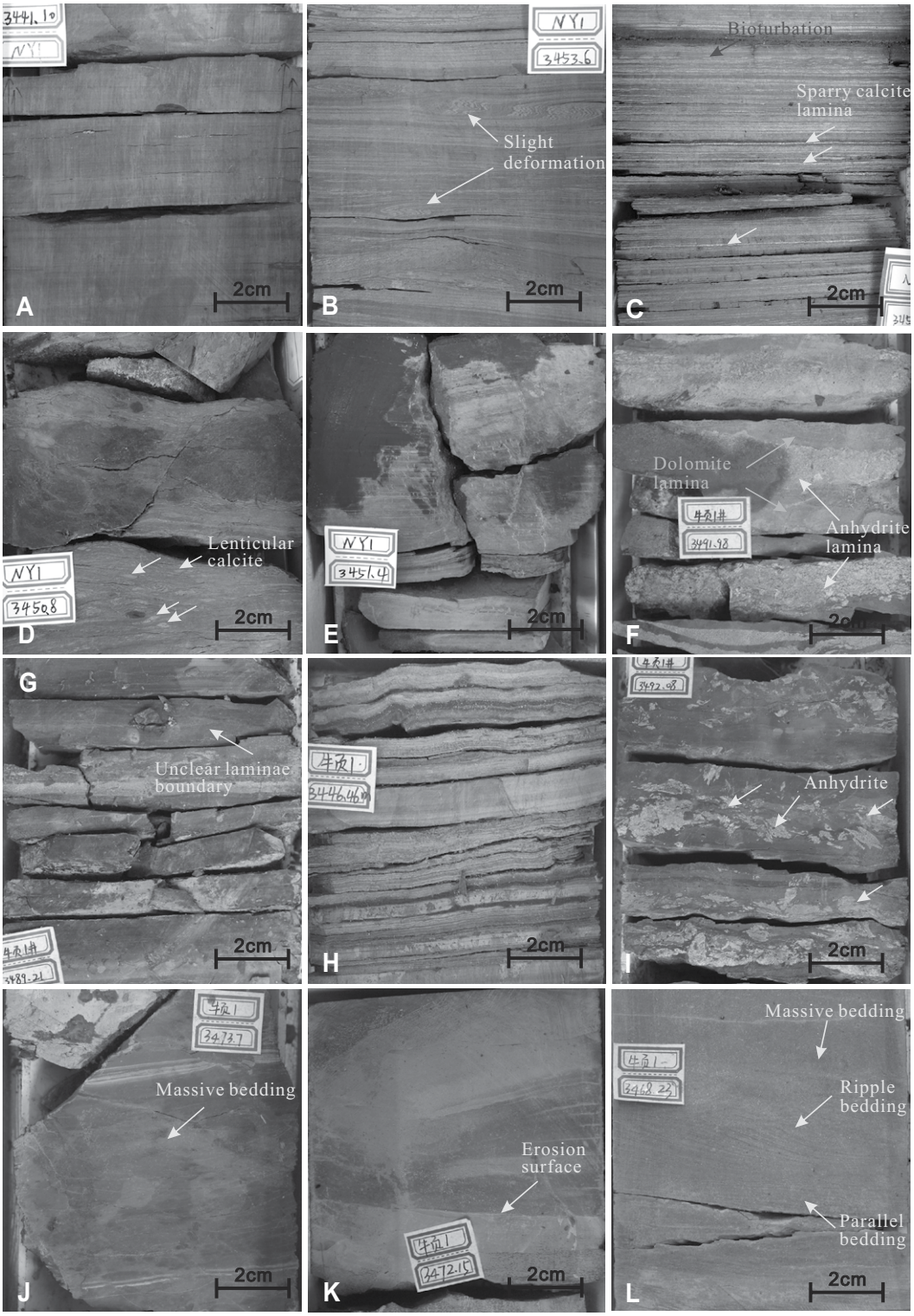

Figure 6. Photographs of cores to show the characteristics of different lithofacies within the lower Es4s shale (depths in brackets). (A) Grayish black laminated calcareous mudstone lithofacies sample with well-preserved and nonbioturbated laminae (well NY1: 3441.10 m. (B) Dark-gray laminated calcareous mudstone lithofacies sample with slight deformation in some laminae (well NY1: 3453.6 m). (C) Dark-gray laminated calcareous mudstone lithofacies sample with well-preserved laminae and clear laminae boundaries. These light laminae contain sparry calcite (well NY1: 3459.06 m). (D) Grayish black laminated calcareous mudstone lithofacies sample containing lenticular calcite and strong deformation (well NY1: 3450.8 m). (E) Gray laminated dolomitic mudstone sample (well NY1: 3451.4 m). (F) Shallow gray laminated dolomitic mudstone sample with thick dolomite laminae and an anhydrite interlayer (well NY1: 3491.98 m). (G) Black laminated clay mudstone sample with a thick and unclear laminae boundary (well NY1: 3489.21 m). (H) Grayish black laminated clay mudstone sample with thin and well-developed laminae (well NY1: 3446.46 m). (I) Gray laminated gypsum mudstone sample with unclear laminae (well NY1: 3492.08 m). (J) Blue-gray massive mudstone sample (well NY1: 3473.7 m). (K) Gray massive mudstone sample showing truncated structure (well NY1: 3472.15 m). (L) Siltstone sample containing massive bedding and ripple lamination (well NY1: 3468.23 m).

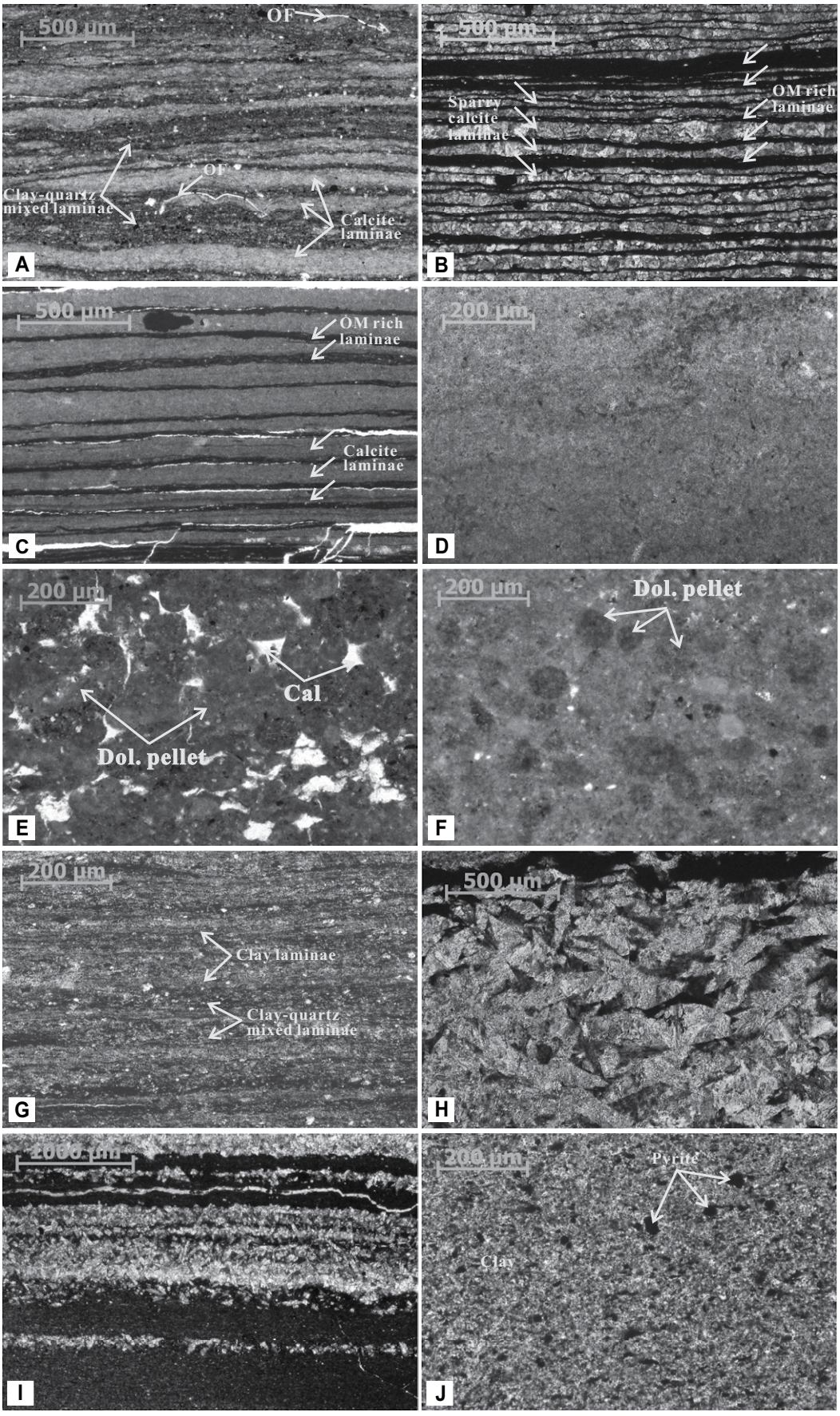

Figure 7. Microscopic characteristics of the different lithofacies that comprise the Es4s shale (depths in parentheses). (A) Sample of laminated calcareous mudstone lithofacies with light micritic calcite laminae containing ostracod fragments (OF) and dark clay-quartz mixed laminae (well NY1: 3453.3 m). (B) Sample of laminated calcareous mudstone lithofacies showing clear boundaries between light sparry calcite and dark organic-rich laminae (well NY1; 3464.89 m). (C) Sample of laminated dolomitic mudstone with well-preserved thick light micritic dolomite and thin dark organic-rich laminae (well NY1: 3466.17 m). (D) Sample of laminated dolomitic mudstone containing micritic dolomite (well NY1: 3475.49 m). (E) Sample of laminated dolomitic mudstone containing algal dolomite (Dol.) pellets cemented by calcite (well NY1: 3485.96 m). (F) Sample of laminated dolomitic mudstone containing algal dolomite pellets floating in micritic dolomite-clay mixed materials (well NY1: 3478.24 m). (G) Sample of laminated clay mudstone containing clay and clay-quartz-feldspar mixed laminae (well NY1: 3481.23 m). (H) High-crystallinity anhydrite in a sample of laminated gypsum mudstone (well NY1: 3496.43). (I) Sample of laminated gypsum mudstone containing light anhydrite and dark clay-rich laminae (well NY1: 3488.56 m). (J) Sample of massive mudstone containing clay minerals, pyrite aggregates (yellow arrows), and scarce large debris pieces (well NY1: 3467.33 m).

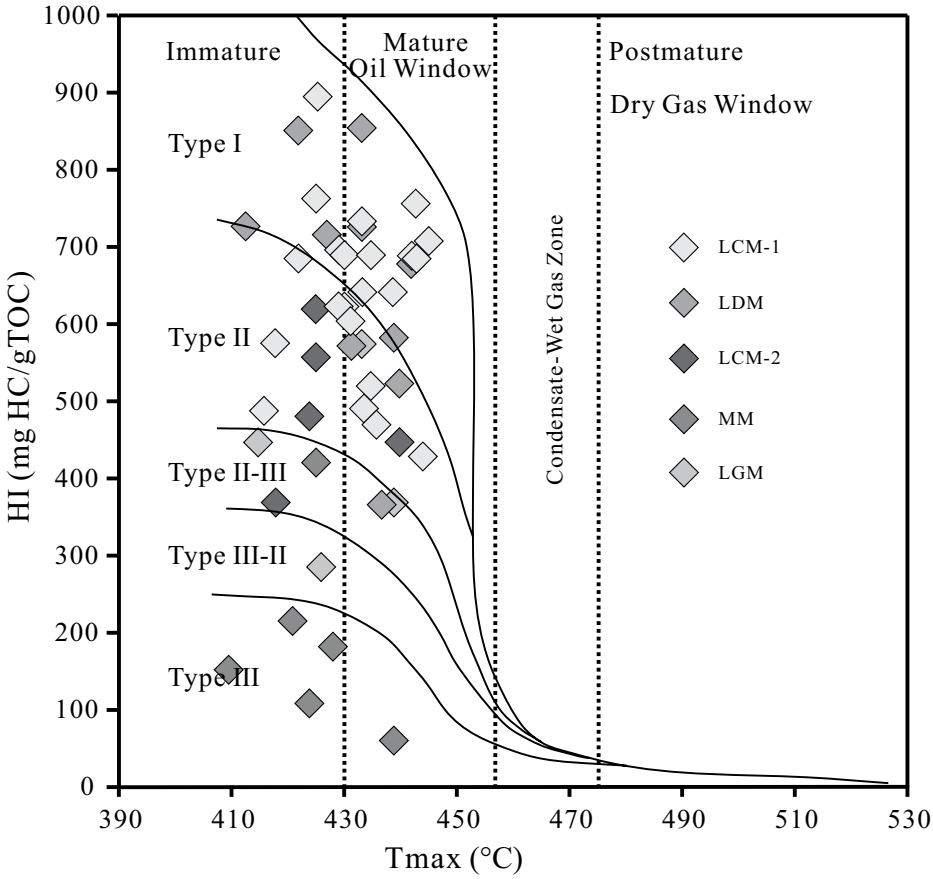

Figure 8. Organic matter types in the different lithofacies of the lower Es4s shale: (1) laminated calcareous mudstone (LCM-1), (2) laminated dolomitic mudstone (LDM), (3) laminated clay mudstone (LCM-2), (4) laminated gypsum mudstone (LGM), and (5) massive mudstone (MM). HI—hydrogen index; TOC—total organic carbon; HC—hydrocarbons.

A plot of HI versus pyrolysis-based Tmax was then used to classify organic matter types, demonstrating the dominant presence of type I and type II kerogens, although a few samples are characterized by type III kerogen (Fig. 8). Organic matter is mainly derived from planktonic algae, including ditch whip algae, coccoliths, and Bohai algae (Liu et al., 2001; Wang, 2012), which explains the dominance of type I and type II kerogens.

TOC Content and Rock-Eval Pyrolysis

The samples of the Es4s shale from well NY1 have TOC contents in the range 0.15 wt% to 4.29 wt% (average: 2.07 wt%), while free hydrocarbons (S1) values range between 0.06 mg/g and 19.07 mg/g (average: 4.52 mg/g). At the same time, hydrocarbons cracked from kerogen (S2) values of samples range between 0.03 mg/g and 25.2 mg/g (average: 7.39 mg/g), and thus values for hydrocarbon generation potential (S1 + S2) range between 0.09mg/g and 45.53 mg/g (average: 16.46 mg/g; Fig. 9; Table 1). In general, the Es4s shale in the Dongying Depression contains a high proportion of organic matter, which is closely related to high paleoproductivity, the warm-humid climate, and the deep-water environment.

The high TOC of the lower Es4s shale is predominantly sapropelinite with subordinate vitrinite. Relationships between the lithofacies suggest that while the laminated calcareous mudstone, laminated clay mudstone, and laminated dolomitic mudstone all have relatively high TOC content (averages all more than 2 wt%; Table 2), they contain almost no vitrinite content compared to the dominant sapropelinite (Fig. 8). In contrast, laminated gypsum mudstone has a relatively low TOC content (average: 0.84 wt%) and contains type II and type III kerogens (Fig. 8), while the massive mudstone is characterized by a low TOC content (0.15 wt% to 0.69 wt%) and abundant vitrinite (Fig. 8; Table 2).

Depositional Environments and Processes

Element Analysis and Sedimentary Environment

A principal component analysis of geochemical data corroborates the stratigraphic features shown in Table 3, while the evolution of the sedimentary sequence recorded by the lower Es4s shale in well NY1 is illustrated in Figure 10. As discussed already, we used a range of geochemical elements as proxies for sedimentary environment, including Sr/Ba and B/Ga ratios as well as a range of biomarkers to estimate paleosalinity, Th/U and Ni/Co ratios to measure anoxic conditions, and Co, Cr, K, Ni, Al, Ti, and Na values as well as the Fe/Mn ratio to determine sediment provenance (Hatch and Leventhal, 1992; Thiry, 2000; Algeo and Maynard, 2004; Ochoa et al., 2013). These data show that the Th/U ratio of the Es4s shale was relatively low on average, varying between 0.36 and 2.83 (average: 1.01). These values are less than 2, rising to above this level in just the interval between 3470 m and 3473 m. Indeed, Th/U and Fe/Mn ratios have been used to reveal the oxidation reducibility of ancient waterbodies, with lower ratios of the former suggesting a stronger reducing environment (Authur and Sageman, 1994; Guo et al., 2011; Ver Straeten et al., 2011; Delpomdor et al., 2013). Previous studies have shown that values of the Th/U ratio greater than 2 provide evidence for an anoxic water body; thus, the low Th/U ratio in the Es4s shale suggests a strongly reducing environment, while this increases in the interval between 3470 m and 3473 m. At the same time, the Sr/Ba ratio varies between 1.7 and 13.02 (average: 5.22), and biomarker data show that the gammacerane index (GI) ranges between 0.5 and 1.8, the Pr/Ph ratios are between 0.2 and 0.8, and the GI/C31 hopane ratio ranges between 1 and 12 (Fig. 11). Generally, a high gammacerane index indicates high paleosalinity. The low Pr/Ph ratio and high GI/C31 hopane ratio reflect high paleosalinity, and, generally, a Pr/Ph ratio lower than 0.8 and GI/C31 hopane ratio higher than 1.0 suggest salinized lake water (Zhu et al., 2005). All these data suggest that the paleolake was saline. However, the Sr/Ba ratio changes cyclically across our study interval, and four anomalously high values occur, reaching 11.18, 9.84, 13.02, and 9.87 at depths of 3454.26 m, 3464.6 m, 3483.3 m, and 3494.82 m, respectively. Because these ratios provide information on salinity variation during sediment deposition (Li and Wang, 1990; Xu et al., 2015), high Sr/Ba values in the Es4s shale suggest the presence of extremely saline lake water, consistent with biomarker data. The lower Es4s shale is characterized by a fine grain size, the scarce presence of large debris

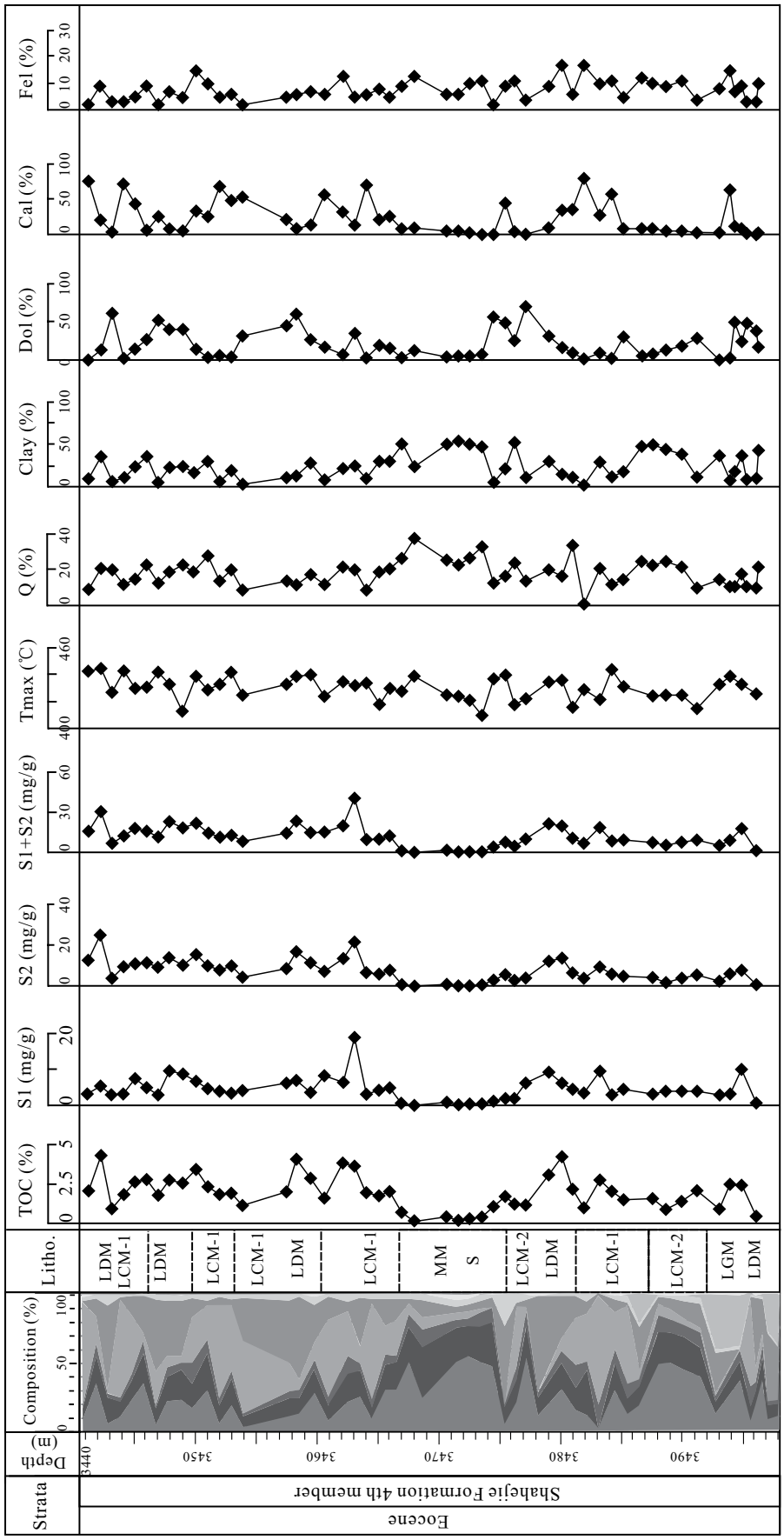

Figure 9. Geochemistry and main mineral composition in the six lithofacies of the lower Es4s shale in well NY1: (1) laminated calcareous mudstone (LCM-1), (2) laminated dolomitic mudstone (LDM), (3) laminated clay mudstone (LCM-2), (4) laminated gypsum mudstone (LGM), (5) massive mudstone (MM), and (6) siltstone (S). Abbreviations: Q—quartz; Dol—dolomite; Cal—calcite; Fel—feldspar; S—siltstone; S1—free hydrocarbons; S2—hydrocarbons cracked from kerogen; Tmax—maximum yield temperature of pyrolysate.

TABLE 3. ELEMENT ANALYSIS OF THE ES4S SHALE IN WELL NY1

Depth (m)	Sr/Ba	Fe/Mn	Mg/Ca	Al (%)	Ba (μg/g)	Ca (%)	Co (μg/g)	Cr (μg/g)	Fe (%)	Ga (μg/g)	K (%)	Mg (%)	Mn (μg/g)	Na (%)	Ni (μg/g)	Sr (μg/g)	Ti (%)	Zn (μg/g)
3439.77	3.32	0.31	0.43	3.32	407.9	18.11	6.61	43.58	2.80	20.78	0.94	7.84	893.7	0.60	131.80	1356	0.15	201.10
3441.87	4.12	0.31	0.20	6.96	360.3	10.30	19.21	65.47	2.56	20.24	1.78	2.06	818.6	1.12	408.80	1483	0.30	112.10
3443.83	4.52	0.09	0.03	2.88	390.4	27.25	6.46	29.26	1.31	33.72	0.83	0.95	1473.0	0.52	17.92	1766	0.12	80.29
3445.78	3.80	0.26	0.44	5.66	250.7	8.42	11.70	39.50	1.77	17.01	1.54	3.67	670.8	1.11	62.55	953	0.26	151.50
3450.32	5.58	0.73	0.29	6.57	202.7	13.26	16.13	56.24	3.34	11.76	1.71	3.82	460.8	1.38	214.60	1131	0.32	122.10
3452.26	3.70	0.16	0.03	1.53	550.6	28.98	4.03	30.38	2.46	33.75	0.46	0.83	1517.0	0.36	13.78	2039	0.07	105.40
3454.26	11.18	0.18	0.36	0.78	177.9	23.19	3.13	0.12	0.79	11.15	0.23	8.40	438.6	0.43	16.18	1989	0.04	311.20
3457.77	8.79	0.32	0.34	2.92	171.7	17.51	6.28	15.76	1.69	13.58	0.87	5.93	533.4	0.70	33.75	1510	0.13	107.00
3459.89	4.33	0.26	0.29	6.17	243.3	12.07	10.12	44.50	2.03	17.91	1.93	3.51	770.2	1.11	638.50	1053	0.30	101.40
3462.58	2.74	0.56	0.14	6.85	351.4	11.34	19.46	78.68	2.78	11.42	1.79	1.56	497.8	1.82	161.30	963	0.31	261.10
3464.60	9.84	0.30	0.03	2.83	371.9	26.91	6.23	32.87	0.95	7.17	0.89	0.79	315.2	0.65	25.67	3660	0.14	78.19
3466.59	5.48	0.39	0.19	5.50	223.0	14.95	11.42	63.39	2.14	11.90	1.77	2.84	543.1	0.84	152.60	1222	0.25	108.20
3468.65	3.16	0.46	0.22	6.59	306.2	5.47	13.80	83.65	3.21	15.32	1.96	1.19	701.0	1.45	33.05	969	0.32	162.80
3472.49	2.97	0.83	0.45	9.01	235.4	2.73	13.28	102.90	2.95	8.13	2.80	1.24	357.2	1.18	132.60	699	0.43	71.62
3474.55	1.70	0.72	1.00	8.72	251.6	1.27	15.91	101.00	2.20	6.52	2.92	1.27	302.8	1.40	286.60	429	0.48	64.39
3476.48	2.69	1.03	0.09	7.55	293.3	8.99	16.18	103.40	2.62	5.94	2.23	0.83	255.8	1.29	391.30	789	0.36	105.10
3478.24	2.67	0.17	0.49	3.18	323.3	15.27	5.55	46.73	1.12	13.87	1.07	7.47	641.6	0.94	251.80	862	0.15	57.05
3481.35	6.00	0.44	0.14	4.45	265.6	14.96	11.43	93.90	2.39	14.76	1.18	2.04	545.8	1.50	82.10	1594	0.22	190.70
3483.30	13.02	0.08	0.01	0.67	546.4	37.15	1.79	27.09	0.20	6.74	0.26	0.52	251.2	0.24	14.82	7112	0.03	69.49
3485.44	6.52	0.26	0.02	1.00	116.9	34.04	3.63	64.23	1.69	18.48	0.26	0.51	655.4	0.52	14.99	762	0.06	130.70
3489.12	3.35	0.37	0.36	6.69	229.5	10.13	11.16	87.82	2.66	17.30	2.35	3.63	728.0	1.13	48.57	768	0.31	65.95
3491.66	3.27	0.26	0.49	5.48	584.7	10.17	11.53	71.21	1.71	16.05	1.84	4.96	664.0	1.28	235.70	1912	0.26	74.89
3494.82	9.87	0.23	0.20	1.07	93.9	21.04	2.66	58.49	0.78	8.75	0.39	4.29	342.6	0.38	54.34	927	0.05	79.27
3496.71	2.75	0.45	0.33	6.64	278.0	8.46	15.89	117.10	1.71	12.44	2.32	2.77	380.6	1.47	149.90	765	0.32	74.20

(i.e., quartz and feldspar grains), and abundant in situ minerals. Generally, terrigenous inputs are weak, and clastic-related elements exhibit a number of weak vertical fluctuations.

In order to further analyze vertical variations in lithofacies associations, paleosalinity, redox properties, and terrigenous inputs, we divided the lower Es4s shale into six intervals from bottom to top, I, II, III, IV, V, and VI.

Interval I (between 3500 m and 3492 m depth). This interval is characterized by high anhydrite content and contains almost all lithofacies of this type. The other components of this interval are mainly dolomite and clay minerals, with subordinate quartz, calcite, and feldspar. As a result, the laminated gypsum mudstone and laminated dolomitic mudstone are the predominant lithofacies in this interval, with interbeds of laminated calcareous mudstone. The geochemical elements that characterize this interval are indicative of relatively high paleosalinity, a strongly reducing environment associated with the water body, and a low proportion of clastic-related elements. All these data suggest limited detrital inputs to the interval, corroborated by the rare detrital minerals.

Interval II (between 3492 and 3487 m depth). Clay minerals, quartz, and feldspar are the dominant minerals in this interval, occurring at significantly higher levels than in interval I. The feldspar, calcite, and dolomite proportions are small, and the laminated clay mudstone is the dominant lithofacies. In this interval, indications of paleosalinity and the reducing level of the water body are less than those seen in interval I, while a slight increase in clastic elements suggests an enhanced proportion of detrital input.

Interval III (between 3487 and 3475 m depth). This interval is characterized by a high proportion of carbonate minerals, and it has a calcite-rich base and a dolomite-rich top. The laminated calcareous mudstone lithofacies and the laminated dolomitic mudstone are the dominant lithofacies, well developed in the lower and upper portions of this interval, respectively. Geochemical analysis suggests that this interval is characterized by generally high paleosalinity, a strongly reduced water body, and limited detrital input. Data show that paleosalinity initially increases before decreasing, and that the transition point delineates the laminated calcareous mudstone lithofacies from the laminated dolomitic mudstone lithofacies.

Interval IV (between 3475 and 3467 m depth). This interval is characterized by high proportions of clay minerals and quartz, as well as rare carbonates, while the massive mudstone is the main lithofacies. The Sr/Ba ratio of this interval is the lowest recorded in the entire lower Es4s shale, suggesting reduced paleosalinity, while Th/U and Th/K ratios suggest oxidation of the water body, and a high proportion of clastic elements suggests enhanced detrital input.

Interval V (between 3467 m and 3453 m depth). This interval is characterized by a high proportion of carbonate minerals as well as subordinate clay and quartz. Similar to interval III, the laminated calcareous mudstone lithofacies and the laminated dolomitic mudstone are the main lithofacies, well developed in the lower and upper portions, respectively. Geochemical analysis suggests that this interval is characterized by a generally high and variable paleosalinity, a strongly reduced water body, and detrital inputs that first increase before subsequently decreasing.

Interval VI (between 3453 m and 3440 m depth). Compared to the other intervals, no single mineral is dominant in interval VI; clay, calcite, and dolomite occur in almost equal proportions. In this interval, laminated calcareous mudstone lithofacies, laminated clay mudstone, and the laminated dolomitic mudstone are interbedded, and geochemical analysis combined with the Sr/Ba ratio are indicative of stable, low-salinity values and few fluctuations. The Th/U and Th/K ratios recorded in this interval suggest a gradually increasing trend toward reduction, while the proportion of clastics is characterized by stable, high values at the base of the interval, decreasing slightly toward the top.

As sediments transition from intervals I to VI, paleosalinity, paleoclimate, degree of reduction, and terrigenous input experience three major cycles, I to II, III to IV, and V to VI. Indeed, from the base of this sequence to the top, each cycle is characterized by a change from high to low salinity, a strong degree of reduction to relatively weak reduction, a drought to humid climate, and strong-to-weak terrigenous input (Fig. 10). The thickness of each interval ranges from several meters to more than 10 m, reflecting high-frequency oscillations in the environment of the lake basin, which are markedly different from a relatively stable marine environment.

Depositional Processes and Model

Analysis of geochemical elements suggests that the lower Es4s shale was deposited in a reduced saline water body environment that had limited terrigenous inputs. This conclusion is corroborated by the fact that the laminated calcareous mudstone lithofacies, laminated dolomitic mudstone lithofacies, and laminated clay

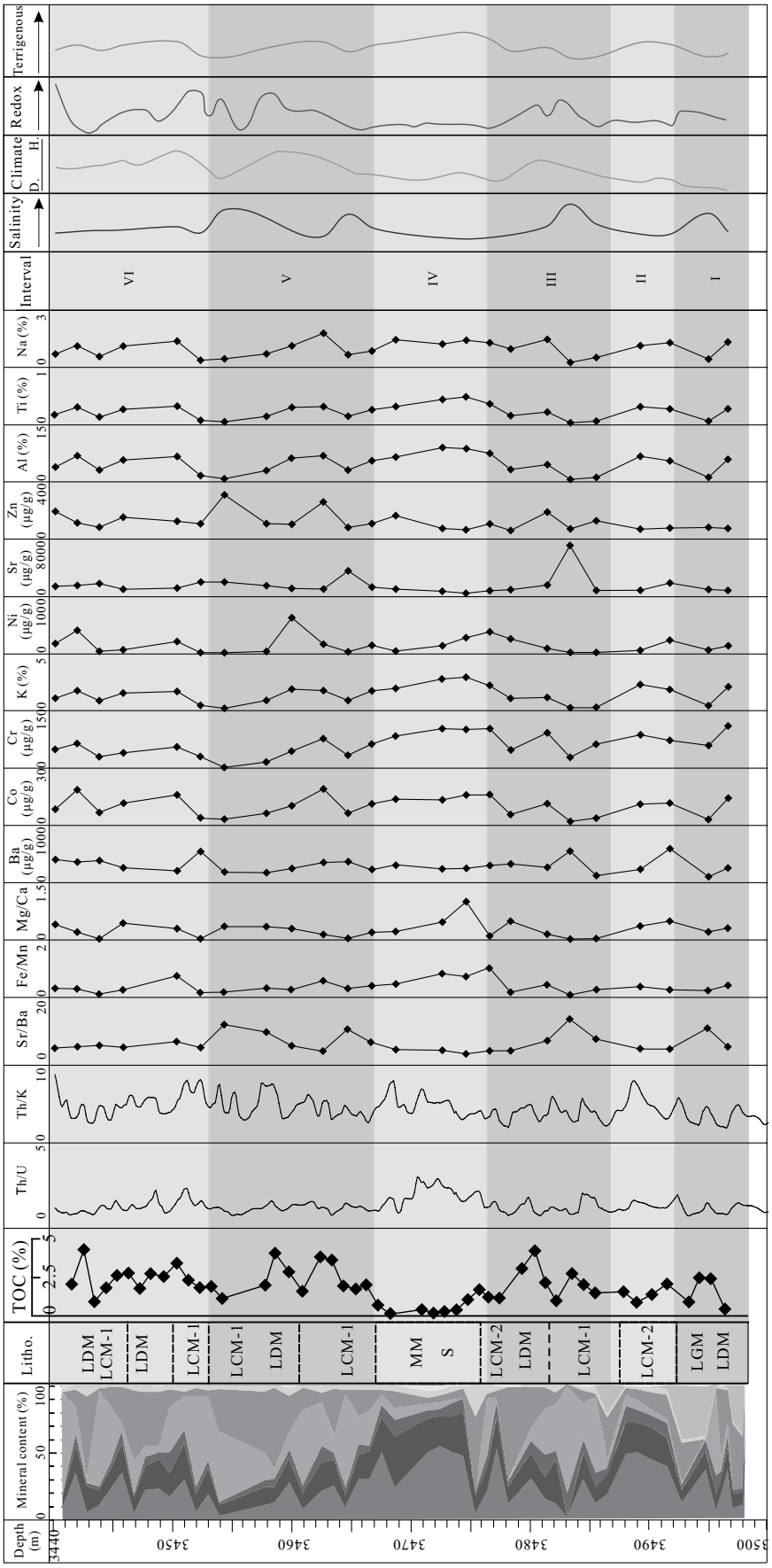

Figure 10. Element analysis of the six lithofacies of the lower Es4s shale in well NY1: (1) laminated calcareous mudstone (LCM-1), (2) laminated dolomitic mudstone (LDM), (3) laminated clay mudstone (LCM-2), (4) laminated gypsum mudstone (LGM), (5) massive mudstone (MM), and (6) siltstone (S). Elements Ba through Na are in ppm. D.—dry; H.—humid.

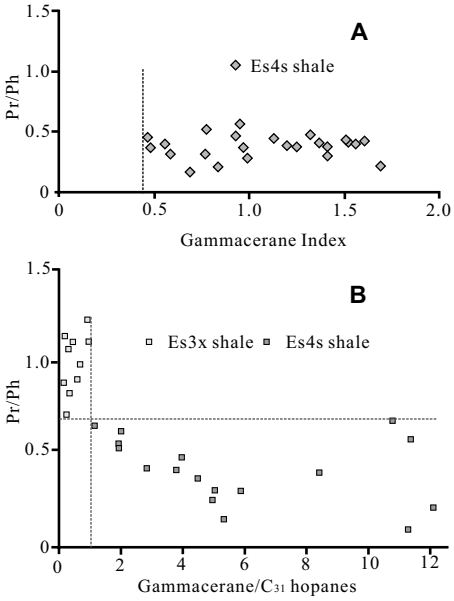

Figure 11. Biomarker characteristics of the Es4s shale. (A) Relationship between the gammacerane index and the Pr/Ph ratio. (B) Relationship between the gammacerane index/C31 hopane ratio and the Pr/Ph ratio.

mudstone lithofacies are all characterized by fine grain sizes, rare large terrigenous debris (i.e., quartz and feldspar), and compositions that are rich in pyrite and sapropelic organic matter (Table 2). These characteristics imply that these lithofacies were mainly deposited out of suspension in a calm water body where there was a relatively low rate of deposition, as corroborated by well-developed organic matter–rich and carbonate-rich laminae (Figs. 7B and 7C).

Laminae characteristics also aid in our understanding of the depositional processes leading to the Es4s shale in the Dongying Depression. As shown in Figure 7A, fragments of ostracods and lenticular carbonate laminae (Fig. 7A) are common in laminated calcareous mudstone lithofacies 1, a lithofacies that has a relatively low TOC content alongside higher clay and quartz contents (Fig. 7A). These characteristics suggest that this lithofacies reflects terrestrial material transport, while, at the same time, the orientations of ostracod fragments and calcareous lenses follow the direction of laminae, suggesting that relatively weak hydrodynamic conditions transported the terrigenous remains. This conclusion is supported by weak deformation within laminae observed the core scale (Fig. 6B); lithofacies that contain lenticular carbonate laminae but lack evidence for terrigenous transport (e.g., ostracod fragments) were likely formed by bioturbation (Fig. 6C). In the organic-rich lithofacies laminated calcareous mudstone lithofacies 1 and laminated dolomitic mudstone, organic matter has been enriched in laminae (Figs. 6B and 6C) that exhibit continuous stable and clear boundaries with their neighboring carbonate laminae (Figs. 6B, 6C, 7B, and 7C). Formation of these laminae was related to cyclical climate change, most likely the result of seasonal climate change, leading to the formation of carbonates in the spring and summer and organic-rich laminae in the fall and winter. This cyclicity has been interpreted to indicate that warm springs and summers contribute to biological blooms, inducing the precipitation of carbonates via changes in water conditions through photosynthesis, followed by the subsequent death of organisms in the autumn and winter.

Laminae are not well developed in the laminated clay mudstone lithofacies; their boundaries are unclear and difficult to distinguish (Fig. 6G), reflecting a relatively stable, long-term depositional environment. Microscopic observations show that these laminae are composed of clay and clay-quartz mixed components (Fig. 7G), with limited compositional differences between laminae. In clay-quartz mixed laminae, detrital quartz is rare, while microcrystalline forms (1 μm to 3 μm) are more common (Figs. 12A and 12B), often wrapped with clay minerals. It is likely that the quartz in these clay-quartz mixed laminae mainly originated from the desiliconization of clay minerals.

The laminated gypsum mudstone lithofacies was likely deposited in an evaporative environment (Li, 1990). Indeed, deposition of the laminated gypsum mudstone would have consumed Ca^{2+} and SO_4^{2-}, increased the Mg^{2+}/Ca^{2+} ratio, and eliminated the dolomite kinetic barrier that promoted deposition of the laminated dolomitic mudstone. The laminated clay mudstone lithofacies was deposited in such a way that it led to an increase in small terrigenous materials, including clay minerals and fine silts. Overall, deposition of these lithofacies was controlled by the geochemistry of the water body, paleoclimate, and terrigenous inputs; laminated mudstones dominate the lower Es4s shale (Fig. 10), suggesting that suspension was the main process of deposition across the study area.

Within the lower Es4s shale, siltstones are characterized by the presence of wavy or horizontal bedding, as well as occurring as interbeds, always with a sharp interface between them and the underlying black shale (Figs. 13A and 13B). In many cases, siltstone is associated with the massive mudstone lithofacies; characteristics of deposition range from wavy and horizontal bedding at siltstone bases to massive mudstone at the top, typical of the C, D, and E sections of the Bouma sequence (Fig. 13). The massive mudstone is characterized by large-scale structures, disorganized and chaotic detrital grains, a low TOC content (0.15 wt% to 0.69 wt%), and a relatively high vitrinite

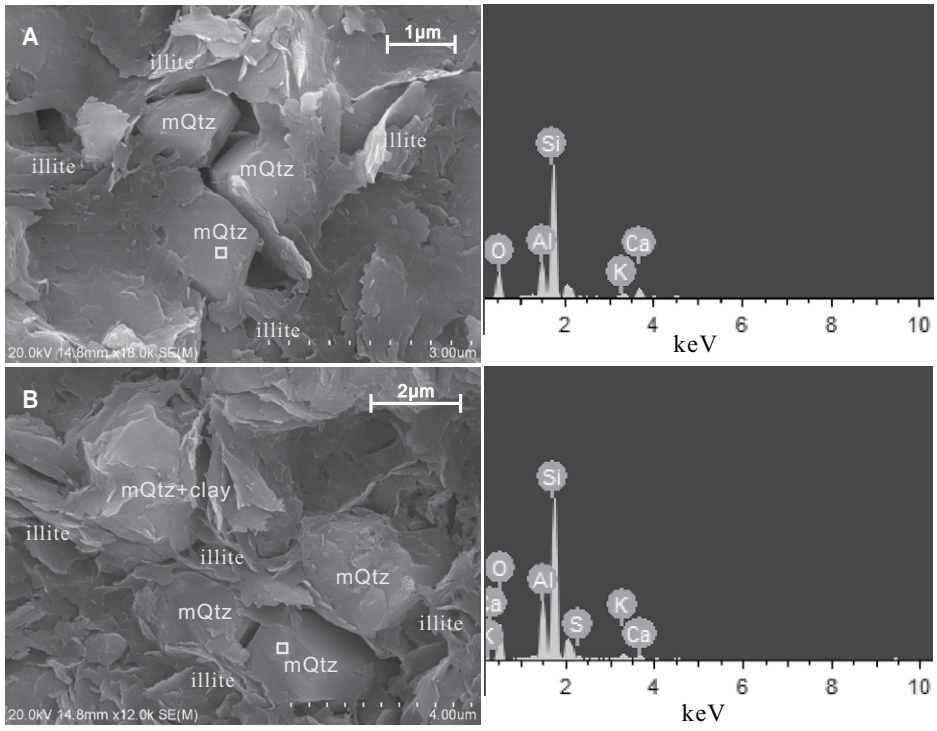

Figure 12. Microcrystalline quartz (mQtz) characteristics of the laminated clay mudstone.

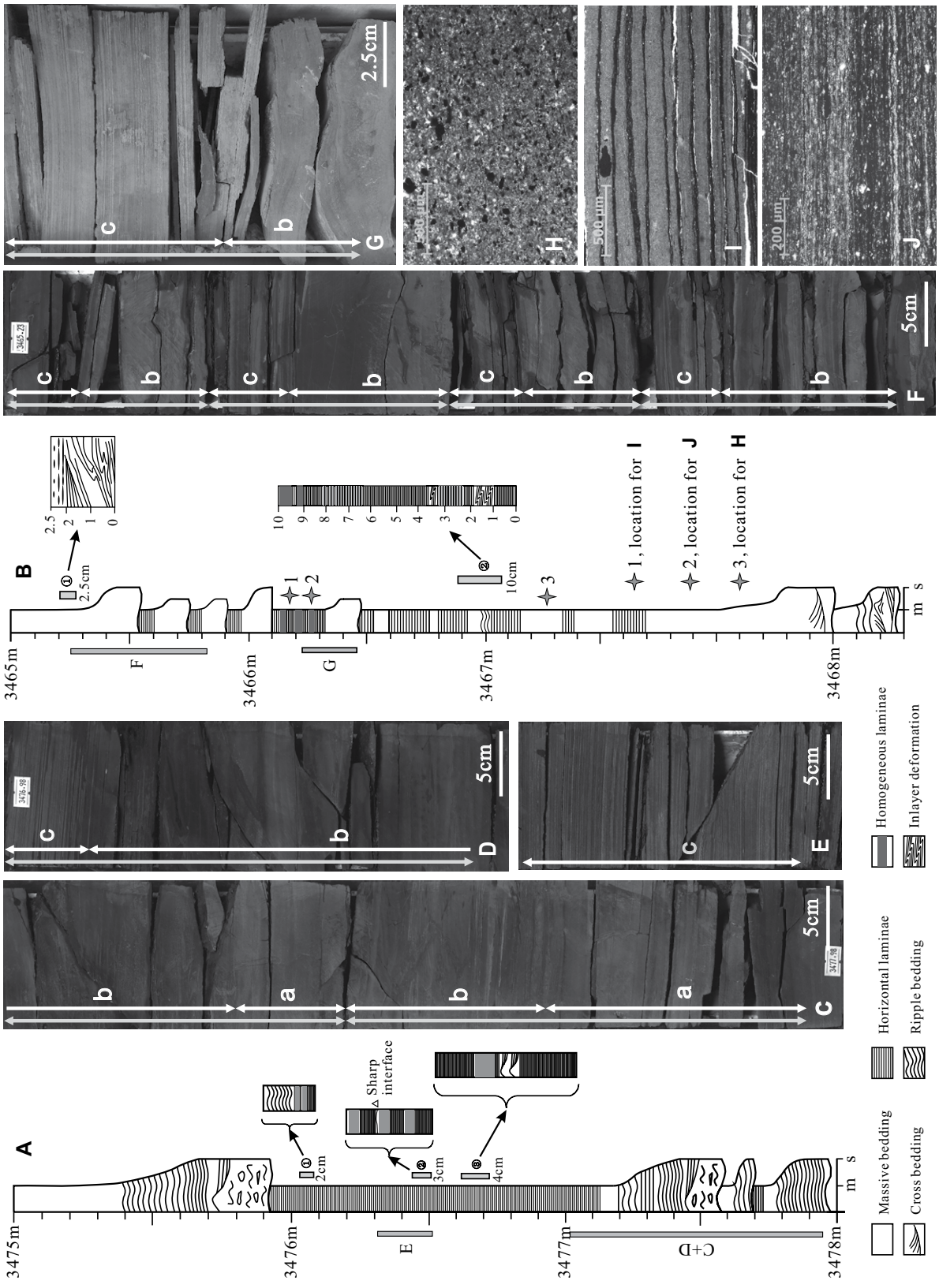

Figure 13. Detailed stratigraphic sections containing descriptions of lithologies and sedimentary structures within the turbidite intervals of the Es4s shale (A) between 3475 m and 3478 m and (B) between 3465 m and 3468.3 m. Unit a—gray siltstone; unit b—massive mudstone; unit c—laminated mudstone. (C–D) Continuous section from 3477.98 m to 3477 m comprising two main cycles: (1) units a and b, and (2) units a, b, and c, with abrupt contact at the bottom of the cycles. (E) Laminated mudstone with horizontal laminae and homogeneous laminae. (F) Cores from 3465.82 m to 3465.23 m comprise four unit b and c cycles and show the abrupt contact at their bases, 15 cm to 20 cm for one cycle. (G) 15 cm thickness of unit b and c cycles, showing the abrupt contact at their bases. Unit c is mainly a laminated mudstone containing homogeneous laminae. (H) Microscopic view of massive mudstone with disorganized and chaotic detrital grains (well NY1: 3467.26 m). (I) Microscopic view of laminated mudstone containing calcareous and organic-rich laminae (well NY1: 3466.17 m). (J) Microscopic view of laminated mudstone containing organic-rich clay laminae (well NY1: 3466.25 m). m—mud; s—silt.

content (Table 2), markedly different from the characteristics of the laminated shale. These massive structures and disorganized detrital grains imply rapid deposition, likely associated with turbidity currents, as evidenced by Bouma section E (Bouma and Stone, 2000). We therefore interpret this siltstone and the associated organic-poor massive mudstone lithofacies as fine-grained turbidites. In sum, we have identified a number of lithofacies types characteristically formed by turbidites across the field area, including siltstones, massive mudstones, and laminated mudstones from bottom to top (Figs. 13C–13E), siltstones and massive mudstones from bottom to top (Fig. 13C), and mudstones and laminated mudstones from bottom to top (Figs. 13F–13J). Our observations suggest that the single layer thickness of turbidite deposition in this area ranges between 0.1 m and 0.5 m (Figs. 13A and 13B), and that these debris-flow currents transported a large amount of O_2 to the lake bottom (Liang et al., 2016), resulting in the oxidation of organic matter and the low TOC content of the massive mudstone. Nevertheless, a relatively high Th/U ratio suggests strong oxidation within the massive mudstone interval (between 3470 m and 3473 m), which differs from the strong reducing tendencies generally associated with the ancient waterbodies across this whole interval (Fig. 10).

Based on data drawn from lithofacies, organisms, and mineral compositions, as well as analysis of sedimentary environments, we interpret that the lower Es4s shale was deposited by suspension in a saline, medium-depth lake that had anoxic bottom water conditions. Deposition of these lithofacies was controlled by the geochemistry of the water body, paleoclimate, and terrigenous inputs. Lithofacies change rapidly up the vertical section (Fig. 14); intervals I, III, and V are characterized by high salinity, low terrestrial input, and strong reducing tendencies,

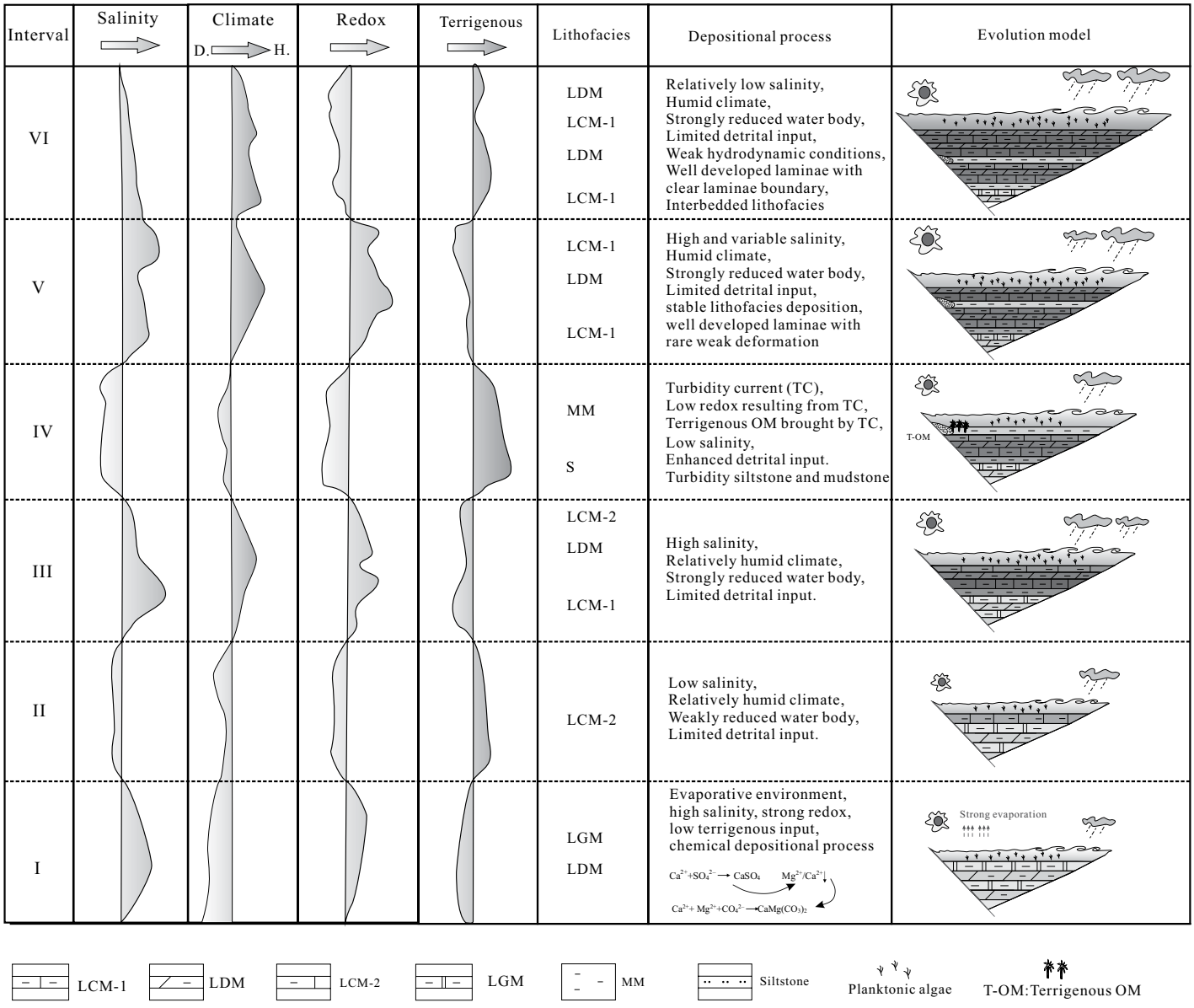

Figure 14. Evolution model of the sedimentary environment and six lithofacies of the lower Es4s shale: (1) laminated calcareous mudstone (LCM-1), (2) laminated dolomitic mudstone (LDM), (3) laminated clay mudstone (LCM-2), (4) laminated gypsum mudstone (LGM), (5) massive mudstone (MM), and (6) siltstone (S). D.—dry; H.—humid; OM—organic matter.

and their lithofacies are dominated by laminated calcareous mudstone lithofacies and laminated dolomitic mudstone, with subordinate interbeds of laminated gypsum mudstone deposited in interval I with evaporative conditions. In contrast, intervals II, IV, and VI are characterized by relatively low salinity, high terrestrial input, and a decreased tendency toward a reducing environment, and the proportions of massive mudstone and laminated clay mudstone lithofacies significantly increase (Fig. 14). The deformation of the laminae is related to the hydrodynamic conditions, which mainly occur in intervals II, IV, and VI, corresponding to increasing terrigenous input. Across this transition, TOC content exhibits the same characteristics as lithofacies changes, suggesting that these high-frequency oscillations in the depositional environment controlled the material composition and organic matter enrichment in the shale. In general, high salinity, warm and humid climate, strong reducing tendencies, and low terrestrial input are important factors that favor the enrichment of organic matter.

Depositional processes included suspension and the movement of turbidity currents, where suspension was the main process leading to deposition of the lower Es4s shale in the study area (Fig. 15). High-salinity conditions were likely related to seawater transgression, as these transport Mg^{2+} and SO_4^{2-}, and precipitation of $CaSO_4$ promotes dolomite formation. Anoxic bottom water conditions would have been disturbed by turbidity currents that transported terrigenous organic material. Thus, all the evidence points to the fact that the lower Es4s shale was formed in a depositional environment consisting of a saline, medium-depth lake, with anoxic bottom water conditions and limited terrigenous input.

DISCUSSION

Mechanism of Salinization

The high Sr/Ba and MgO/Al_2O_3 ratios recorded in the Es4s shale suggest extraordinarily saline lake water. In addition, four anomalously high Sr/Ba values were also recorded, suggesting periods of salinization as the paleosalinity of lake water at the time of formation of the lower Es4s shale reached the range 22‰ to 32‰ (Li and Xiao, 1988). During this interval, average dolomite content reached 21.58 wt%, also anomalously high, while it was just 8.13 wt% at other times. This rapid salinization and corresponding high dolomite accumulation cannot reasonably be interpreted as the result of a drought climate, reduced freshwater input, or terrigenous salts. Indeed, because of the absence of large communicating faults, the lake became very saline at these times (Yuan et al., 2006; Lin et al., 2009). In addition, the interpretation of these fluctuations as the result of weak volcanic and magmatic activity during the formation of the Es4s shale is thought to be inaccurate (Wu et al., 2014).

We also observed the presence of glauconite and foraminifera in thin sections within the lower Es4s shale (Fig. 16). Foraminifera mainly included single-column shells with thin walls that showed evidence of pyritization (Figs. 16C and 16D). Marine planktonic fossils including dinoflagellates and calcareous algae have been found by other workers in corresponding intervals, while O and C isotopic values and the distribution of n-alkanes are also indicative of marine features.

Influence of Seawater Input

Seawater contains abundant salt ions and would lead to a massive increase in lake salinity. Current ocean salinity is ~35‰, higher than most lakes, including Qinghai Lake (12.5‰), the largest inland saltwater lake in China, as well as the Caspian Sea (12.8‰). Previous studies have suggested that salinity reached 32‰ during formation of the Es4s shale, but just 20.6‰ and between 12.6‰ and 15‰ in the semideep lake environment during formation of the Es3x and Es1 units, respectively (Li and Xiao, 1988; Liu, 1998; Yuan et al., 2006). Thus, seawater inputs caused paleosalinity to rapidly increase, as evidenced by abnormal increases in Sr/Ba and Ca/Mg ratios (Fig. 10). At the same time, these inputs diluted terrigenous element concentrations and reduced Mn and Fe proportions significantly in the seawater-

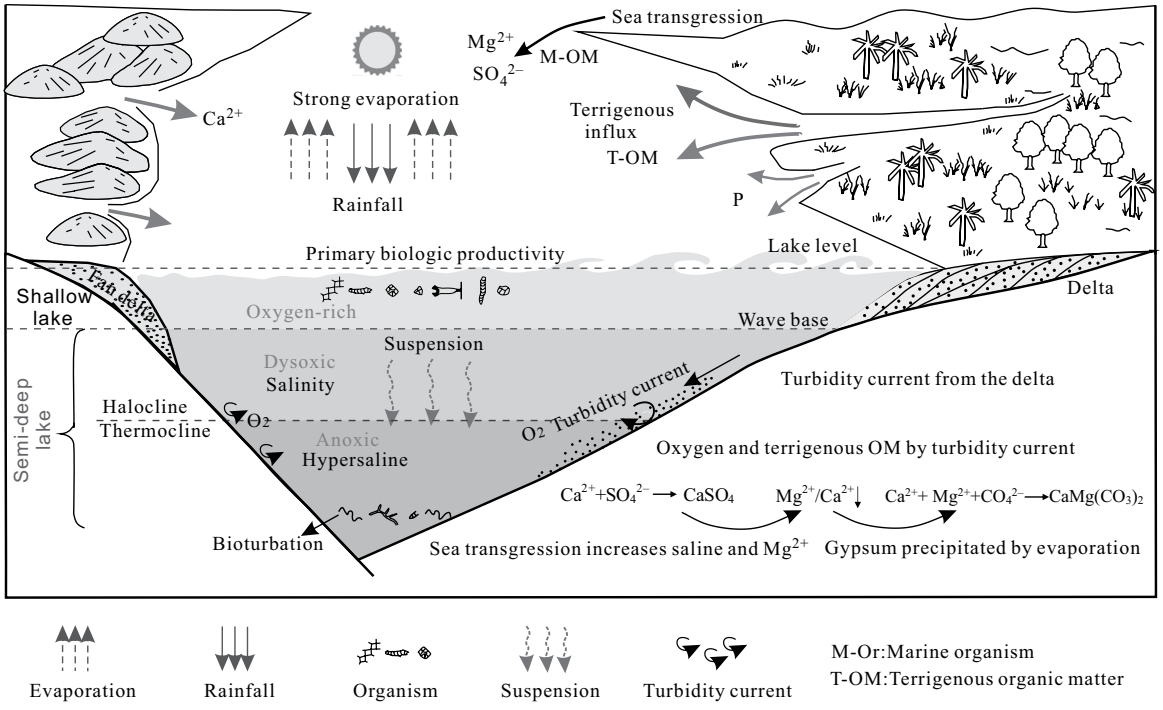

Figure 15. Depositional model for the lower Es4s shale as a semiclosed, medium-depth lake containing anoxic and hypersaline water.

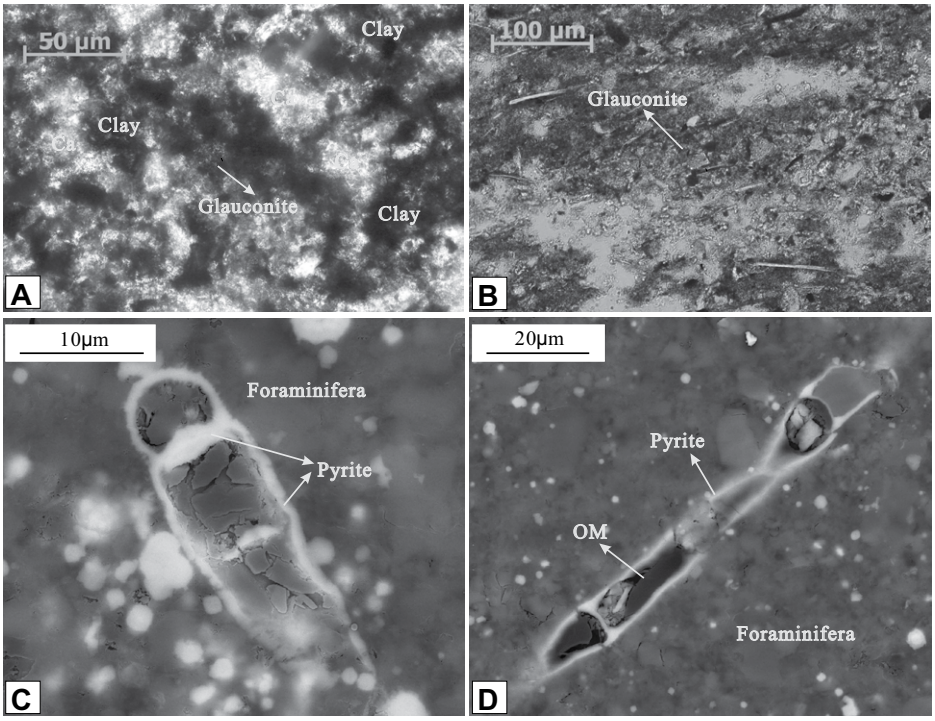

Figure 16. (A) Glauconite in the Es4s shale (well FY1: 3308.4 m). (B) Glauconite in the Es4s shale (well C11: 2323.18 m). (C–D) Examples of foraminifera from the Es4s shale in the size range 50 μm to 100 μm with pyritized shells and organic matter (OM) contents (dark color; well LY1: 3808.95 m).

affected interval. In addition, contents of the trace elements Cr, Co, K, and Ti all exhibit high-amplitude shock features during the seawater-affected interval, reflecting the complex effects of seawater input in changing water properties. Over time, paleosalinity gradually decreased as the result of constant inflow from rivers and atmospheric freshwater, and abnormal trace element values decreased significantly. In addition, the proportions of Fe, Mn, and other elements from terrigenous sources increased significantly, suggesting that transgressive incidents gradually slowed, or even stopped altogether. The rapid rise in the lake level and the increase in paleosalinity caused by the seawater input resulted in anoxic bottom water conditions in the lake and favored the preservation of organic material.

However, compared with other intervals, the period of seawater input is also characterized by a relatively high dolomite content (average: 21.58 wt%), much higher than during normal intervals (8.13 wt%). Dolomite is seen in two forms, the first of which is as bright crystals symbiotic with gypsum, and closely related to its precipitation. The process of gypsum precipitation consumes Ca^{2+} and SO_4^{2-} and leads to an increase in the Mg^{2+}/Ca^{2+} ratio, eliminating the dolomite kinetic barrier. The second form is psammitic dolomite; while the former is poor in organics, the latter has a relatively high TOC content, generally greater than 2 wt%. At the same time, fossils of marine organisms are common, including foraminifera that have pyritized shells and calcispheres. Thus, a high dolomite content may be related to a high proportion of Mg^{2+} in seawater; generally, the Mg^{2+} content of seawater is 260 times that of lake water and 300 times that of river water (Tian et al., 1988; Yuan et al., 2006). Thus, an abundance of Mg^{2+} from seawater would lead to conditions conducive to dolomite precipitation (Hsü and Siegenthaler, 1969; Land, 1991). Compared with lake water, seawater also has a relatively high density and will sink in freshwater (He et al., 2010; Wu et al., 2014); as a result, seawater inputs will lead to stratified lake water chemistry, further resulting in vertical convective circulation, and reducing conditions in lake bottom waters (Zhu et al., 2005; Wang, 2012; Yuan et al., 2015). Seawater is also alkaline, while freshwater and lake waters tend to be acidic; mixing of seawater with lake water will adjust the pH of lake water and lead to slightly alkaline conditions, which would be required for dolomite precipitation (Hardie, 1991; Tucker, 2001; Davies and Smith, 2006). Intrusion of seawater further makes environmental conditions conducive to the removal of the kinetic and thermodynamic barriers associated with dolomite precipitation.

The thick blue-gray massive mudstones in the study area associated with siltstones are of turbidite origin and are characterized by massive bedding, low TOC contents, and disorganized and chaotic detrital grains. Because turbidity was a large-scale and multistage phenomenon across this area, leading to total bed thickness of up to 10 m, this implies frequent turbidite-flow events during the seawater input interval that did not affect the subsequent 200 m thickness of shale. A turbidite needs a triggering mechanism, and seawater input would have provided the conditions necessary to trigger this depositional event.

Potential Reasons Underlying the Input of Seawater

Evidence from petrology, geochemistry, and paleontology suggests that the Dongying Depression was influenced by seawater during deposition of the lower Es4s shale. However, although there is no direct evidence confirming the mechanism for this seawater intrusion, we discuss global climate change as well as plate movements in our search for potential reasons.

Climate change studies have shown that a global, large-scale warming event occurred subsequent to the early-to-mid-Eocene cooling event at ca. 45 Ma, and lasted between 2 and 3 m.y. (Ivany et al., 2008; Tindall et al., 2010; Allen et al., 2015). Because this global warming event coincides temporally with deposition of the Es4s shale, this sequence might represent a sedimentary response to a change in global temperature. Indeed, because the Bohai Bay Basin is a near-ocean inland lake, global warming in the early Eocene leading to a rise in sea level might also present a mechanism for the influx of seawater. Tectonic analysis of East Asia has shown that before the Eocene (ca. 42 Ma), as the Yangtze plate formed a wedge with the North China plate and as subduction of the Pacific plate occurred to the northwest, sinistral strike-slip movement of north-northwest–trending Tanlu fault belts resulted in a sinistral shear stress field to the west (Wu and Liu, 2004; Li et al., 2013; Wu et al., 2014). In addition, tectonic patterns in the western Pacific underwent a fundamental turning point ca. 42 Ma (Suo et al., 2012); as a result of the disappearance of the Kula plate, subduction of the Pacific plate switched from a north-northwest to a northwest-north orientation, the Japanese archipelago began to split off from the East Asian mainland, and Tanlu fault belts began to experience dextral strike-slip movements (Li et al., 2013). Because this transformation in the large-scale tectonic framework

of East Asia during the Eocene coincides with deposition of the lower Es4s shale, we speculate that it likely prompted seawater input. A rise in sea level caused by global warming in the early Eocene together with the large-scale tectonic activity prompted the seawater input.

Organic Matter Accumulation in Black Shale

Conditions beneficial for the accumulation and preservation of organic matter are prerequisites for the formation of high-quality source rocks, and they are related to primary productivity and oxidizing-reducing conditions. Thus, depositional environment, related to the primary productivity of organisms as well as oxidizing-reducing conditions, plays an important role in the accumulation and preservation of organic matter (Arthur and Sageman, 1994; Stow et al., 2001). Abundant organic matter, reflected in high TOC content, in the lower Es4s shale is indicative of high primary productivity. However, because this organic matter is mainly composed of sapropelinite, with little terrestrial organic input, source organisms were mainly planktonic algae, including dinoflagellates, coccolithophores, calcareous algae, and foraminifera. Algal blooms, the predominant primary producers of organic matter in the lower Es4s shale, were likely related to abundance of nutrients and a humid, warm paleoclimate, as evidenced by the Th/K ratio. Studies suggest that the accumulation of organic matter in sediment is also influenced by sedimentation rate. A lower rate is thought to favor organic matter degradation during settling in the water column under oxidizing conditions, while high sedimentation rate can dilute organic matter content in a reducing setting (Stow and Mayall, 2000; Tyson, 2001). The presence of laminated mudstones reflects a low sedimentation rate leading to deposition of the lower Es4s shale, an important control on organic matter accumulation. In addition, the depositional process should be considered as we discuss the relationship between sedimentation rate and organic matter accumulation. Turbidity currents may transport a large amount of O_2 to the lake bottom, resulting in the oxidation of organic matter (Liang et al., 2016). As mentioned, parts of the Es4s lacustrine shale were deposited by biochemical processes, which are different from siliciclastic marine shales. The C and O isotope analysis combined with basin tectonic analysis showed that the Dongying Depression was a closed lake during formation of the Es4s shale (Liu, 1998; Sheng et al., 2008; Wu et al., 2014); high salinity caused layering in the lake water chemistry, resulting in vertical convective circulation and the presence of reducing conditions in the bottom waters, conducive to the preservation of organic matter. A medium-depth lake environment with relatively high salinity, strong stratification of water layers, and anoxic conditions led to favorable preservation conditions for organic matter.

CONCLUSIONS

The results of this study show that the Es4s shale is mainly dominated by carbonates, clay minerals, and quartz, with the former comprising up to 80 wt% (average: 43.67 wt%). We identified six lithofacies as the result of this study, laminated calcareous mudstone, laminated dolomitic mudstone, laminated clay mudstone, laminated gypsum mudstone, massive mudstone, and siltstone. The laminated mudstones were deposited out of suspension in a calm water body at a relatively low rate. Laminated gypsum mudstones were likely deposited in an evaporative environment; their deposition consumed Ca^{2+} and SO_4^{2-} and promoted the deposition of laminated dolomitic mudstone. The laminated clay mudstone lithology was deposited in such a way that the amount of small terrigenous materials was increased, while massive mudstones were likely deposited in a rapid depositional environment associated with siltstone as part of fine-grained turbidite sequences. Our data suggest that the lower Es4s shale was formed in a depositional environment consisting of a saline, medium-depth lake, under anoxic conditions with limited terrigenous input. In addition, the depositional environment of the lake basin was characterized by high-frequency oscillations, which are markedly different from a relatively stable marine environment. This depositional process included suspension as well as the presence of turbidity currents, while high salinity was related to seawater transgression, which affected the lithofacies, triggered turbidity currents, and prompted the accumulation of organic matter. A rise in sea level caused by global warming in the early Eocene together with the large-scale tectonic activity of East Asia promoted the seawater input. The deposition of the Es4s shale in the Dongying Depression help in understanding the deposition of lacustrine shale, paleoclimate reconstructions during the Eocene, and the tectonic activity of East Asia.

ACKNOWLEDGMENTS

The research presented in this paper was supported by the National Natural Science Foundation of China (grants 41690130, 41602142 and 41372107), a Certificate of China Postdoctoral Science Foundation grant (2017T100523 and 2015M582165), and the Natural Foundation of Shandong Province (grant ZR2016DB16). We are grateful to the Geoscience Institute of the Shengli Oilfield, SINOPEC, for granting access to their in-house database.

REFERENCES CITED

Abouelresh, M.O., and Slatt, R.M., 2012, Lithofacies and sequence stratigraphy of the Barnett Shale in east-central Fort Worth Basin, Texas: American Association of Petroleum Geologists Bulletin, v. 96, p. 1–22, doi:10.1306/04261110116.

Algeo, T.J., and Maynard, J.B., 2004, Trace-element behavior and redox facies in core shales of Upper Pennsylvanian Kansas-type cyclothems: Chemical Geology, v. 206, p. 289–318, doi:10.1016/j.chemgeo.2003.12.009.

Allen, S.E., Stull, G.W., and Manchester, S.R., 2015, Icacinaceae from the Eocene of western North America: American Journal of Botany, v. 102, p. 725–744, doi:10.3732/ajb.1400550.

Andersson, P.O.D., and Worden, R.H., 2004, Mudstones of the Tanqua Basin, South Africa: An analysis of lateral and stratigraphic variations within mudstones, and a comparison of mudstones within and between turbidite fans: Sedimentology, v. 51, p. 479–502, doi:10.1111/j.1365-3091.2004.00633.x.

Aplin, A.C., and Macquaker, J.H.S., 2011, Mudstone diversity: Origin and implications for source, seal, and reservoir properties in petroleum systems: American Association of Petroleum Geologists Bulletin, v. 95, p. 2031–2059, doi:10.1306/03281110162.

Aplin, A.C., Macquaker, J.H.S., and Fleet, A.J., 1999, Muds and Mudstones: Physical and Fluid-Flow Properties: Geological Society, London, Special Publication 158, 190 p.

Arthur, M.A., and Sageman, B.B., 1994, Marine black mudstones: Depositional mechanism and environments of ancient deposits: Annual Review of Earth and Planetary Sciences, v. 22, p. 499–551, doi:10.1146/annurev.ea.22.050194.002435.

Bouma, A.H., and Stone, C.G., eds., 2000, Fine-Grained Turbidite Systems: American Association of Petroleum Geologists Memoir 72, 342 p.

Bowker, K.A., 2007, Barnett Shale gas production, Fort Worth Basin: Issues and discussion: American Association of Petroleum Geologists Bulletin, v. 91, p. 523–533, doi:10.1306/06190606018.

Burton, D., Woolf, K., and Sullivan, B., 2014, Lacustrine depositional environments in the Green River Formation, Uinta Basin: Expression in outcrop and wireline logs: American Association of Petroleum Geologists Bulletin, v. 98, p. 1699–1715, doi:10.1306/03201413187.

Butterworth, P.J., and Wain, A.S., 1995, Lowstands and highstands in the lacustrine brown shale of central Sumatra: Field examples from the Teso block, *in* 24th Annual Convention Proceedings: Jakarta, Indonesia, Indonesian Petroleum Association, Volume 2, p. 577.

Cheel, R.J., 1990, Horizontal lamination and the sequence of bed phases and stratification under upper-flow-regime conditions: Sedimentology, v. 37, p. 517–529, doi:10.1111/j.1365-3091.1990.tb00151.x.

Davies, G.R., and Smith, L.B., Jr., 2006, Structurally controlled hydrothermal dolomites reservoir facies: An overview: American Association of Petroleum Geologists Bulletin, v. 90, p. 1641–1690, doi:10.1306/05220605164.

Delpomdor, F., Linnemann, U., Boven, A., Gärtner, A., Travin, A., Blanpied, C., and Préat, A., 2013, Depositional age, provenance, and tectonic and palaeoclimatic settings of the late Mesoproterozoic–middle Neoproterozoic Mbuji-Mayi Supergroup, Democratic Republic of Congo: Palaeogeography, Palaeoclimatology, Palaeoecology, v. 389, p. 4–34, doi:10.1016/j.palaeo.2013.06.012.

Ding, L., Xu, Q., Yue, Y., and Li, S., 2014, The Andean-type Gangdese Mountains: Paleoelevation record from the Paleocene-Eocene Linzhou Basin: Earth and Planetary Science Letters, v. 392, p. 250–264, doi:10.1016/j.epsl.2014.01.045.

Frébourg, G., Ruppel, S.C., Loucks, R.G., and Lambert, J., 2016, Depositional controls on sediment body architecture in the Eagle Ford/Boquillas system: Insights from outcrops in west Texas, United States: American Association of Petroleum Geologists Bulletin, v. 100, p. 657–682, doi:10.1306/12091515101.

Ghadeer, S.G., and Macquaker, J.H.S., 2011, Sediment transport processes in an ancient mud-dominated succession: A comparison of processes operating in marine offshore settings and anoxic basinal environments: Journal of the Geological Society [London], v. 168, p. 1121–1132, doi:10.1144/0016-76492010-016.

Guo, L., Jiang, Z.X., Zhang, J.C., and Li, Y.X., 2011, Paleoenvironment of Lower Silurian black mudstone and its significance to the potential of shale gas, southeast of Chongqing, China: Energy Exploration & Exploitation, v. 29, p. 597–616, doi:10.1260/0144-5987.29.5.597.

Guo, X.W., He, S., Liu, K.Y., Song, G.Q., Wang, X.J., and Shi, Z.S., 2010, Oil generation as dominant overpressure mechanism in the Cenozoic Dongying Depression, Bohai Bay Basin, China: American Association of Petroleum Geologists Bulletin, v. 94, p. 1859–1881, doi:10.1306/05191009179.

Hardie, L.A., 1991, On the significance of evaporates: Annual Review of Earth and Planetary Sciences, v. 19, p. 131–168, doi:10.1146/annurev.ea.19.050191.001023.

Hatch, J.R., and Leventhal, J.S., 1992, Relationship between inferred redox potential of the depositional environment and geochemistry of the Upper Pennsylvanian (Missourian) Stark Shale Member of the Dennis Limestone, Wabaunsee County, Kansas, U.S.A.: Chemical Geology, v. 99, p. 65–82, doi:10.1016/0009-2541(92)90031-Y.

He, Y.L., Liu, B., and Qin, S., 2010, Study on dolomitization and dolostone genesis: Acta Scientiarum Naturalium Universitatis Pekinensis, v. 46, p. 1010–1021 [in Chinese with English abstract].

Hill, R.J., Jarvie, D.M., Zumberge, J., Henry, M., and Pollastro, R.M., 2007, Oil and gas geochemistry and petroleum systems of the Fort Worth Basin: American Association of Petroleum Geologists Bulletin, v. 91, p. 445–473, doi:10.1306/11030606014.

Hsü, K.J., and Siegenthaler, C., 1969, Preliminary experiments on hydrodynamic movement induced by evaporation and bearing on the dolomite problem: Sedimentology, v. 12, p. 11–25, doi:10.1111/j.1365-3091.1969.tb00161.x.

Ivany, L.C., Lohmann, K.C., Hasiuk, F., Blake, D.B., Glass, A., Aronson, R.B., and Moody, R.M., 2008, Eocene climate record of a high southern latitude continental shelf: Seymour Island, Antarctica: Geological Society of America Bulletin, v. 120, p. 659–678, doi:10.1130/B26269.1.

Jarvie, D.M., Hill, R.J., Ruble, T.E., and Pollastro, R.M., 2007, Unconventional shale-gas systems: The Mississippian Barnett Shale of north-central Texas as one model for thermogenic shale-gas assessment: American Association of Petroleum Geologists Bulletin, v. 91, p. 475–499, doi:10.1306/12190606068.

Jiang, X.F., 2011, Main controlling factors of lacustrine carbonate deposition in Jiyang Depression: Petroleum Geology and Recovery Efficiency, v. 18, p. 24–30 [in Chinese with English abstract].

Jiang, Z.X., Liu, H., Zhang, S.W., Su, X., and Jiang, Z.L., 2011, Sedimentary characteristics of large-scale lacustrine beach-bars and their formation in the Eocene Boxing Sag of Bohai Bay Basin, East China: Sedimentology, v. 58, p. 1087–1112, doi:10.1111/j.1365-3091.2010.01196.x.

Jiang, Z.X., Liang, C., Wu, J., Zhang, J.G., Zhang, W.Z., Wang, Y.S., Liu, H.M., and Chen, X., 2013, Aspects of sedimentological studies on oil/gas bearing fine-grained sedimentary rocks: Acta Petrolei Sinica, v. 34, p. 1–9 [in Chinese with English abstract].

Konitzer, S.F., Davies, S.J., Stephenson, M.H., and Leng, M.J., 2014, Depositional controls on mudstone lithofacies in a basinal setting: Implications for the delivery of sedimentary organic matter: Journal of Sedimentary Research, v. 84, p. 198–214, doi:10.2110/jsr.2014.18.

Kuang, L.C., Tang, Y., Lei, D.W., Chang, Q.S., OuYang, M., Hou, L.H. and Liu, D.G., 2012, Formation conditions and exploration potential of tight oil in the Permian saline lacustrine dolomitic rock, Junggar Basin, NW China: Petroleum Exploration and Development, v. 39, p. 700–711, doi:10.1016/S1876-3804(12)60095-0.

Land, L.S., 1991, Dolomitization of the Hope Gate Formation (North Jamaica) by seawater: Reassessment of mixing zone dolomite, *in* Taylor, H.P. Jr., O'Neil, J.R., and Kaplan, I.R., eds., Stable Isotope Geochemistry: A Tribute to Samuel Epstein: Geochemical Society Special Publication 3, p. 121–133.

Li, B.X., 1990, Study on modern continental evaporites: Geochimica, v. 4, p. 333–339 [in Chinese with English abstract].

Li, C.F., and Xiao, J.F., 1988, The application of trace element to the study on paleosalinities in Shahejie Formation of Dongying Depression, Shengli Oil Field: Acta Sedimentologica Sinica, v. 6, p. 100–107 [in Chinese with English abstract].

Li, J.R., and Wang, S.M., 1990, Study of mudstone geochemistry in several bearing oil and gas closed basin, East China: Journal of Lake Sciences, v. 1, p. 1–4 [in Chinese with English abstract].

Li, L., Zhong, D.K., and Shi, M.X., 2007, Cenozoic uplifting/subsidence coupling between the west Shandong Rise and the Jiyang Depression, northern China: Acta Geologica Sinica, v. 81, p. 1215–1228 [in Chinese with English abstract].

Li, S.Z., Yu, S., Zhao, S.J., Liu, X., Gong, S.Y., Suo, Y.H., Dai, L.M., Ma, Y., Xu, L.Q., Cao, X.Z., Wang, P.C., Sun, W.J., Yang, C., and Zhu, J.J., 2013, Tectonic transition and plate reconstructions of the east Asian continental margin: Marine Geology & Quaternary Geology, v. 33, p. 65–94 [in Chinese with English abstract], doi:10.3724/SP.J.1140.2013.03065.

Liang, C., Jiang, Z.X., Cao, Y.C., Wu, M.H., Guo, L., and Zhang, C.M., 2016, Deep-water depositional mechanisms and significance for unconventional hydrocarbon exploration: A case study from the Lower Silurian Longmaxi shale in the southeastern Sichuan Basin: American Association of Petroleum Geologists Bulletin, v. 100, p. 773–794, doi:10.1306/02031615002.

Lin, Z.L., Wang, H., Jiang, H., Yue, Y., Xiao, G.Q., and Zhang, B., 2009, The association analysis of tectonic stress field on episodic rifting in Cenozoic of Beitang Sag of Bohai Bay Basin: Journal of Oil and Gas Technology, v. 31, p. 24–29 [in Chinese with English abstract].

Liu, B., Lv, Y.F., Meng, Y.L., Li, X.N., Guo, X.B., Ma, Q., and Zhao, W.C., 2015, Petrologic characteristics and genetic model of lacustrine lamellar fine-grained rock and its significance for shale oil exploration: A case study of Permian Lucaogou Formation in Malang sag, Santanghu Basin, NW China: Petroleum Exploration and Development, v. 42, p. 656–666, doi:10.1016/S1876-3804(15)30060-4.

Liu, C.L., 1998, Carbon and oxygen isotopic compositions of lacustrine carbonates of the Shahejie Formation in the Dongying Depression and their paleolimnological significance: Acta Sedimentological Sinica, v. 16, p. 109–114 [in Chinese with English abstract].

Liu, C.L., Xu, J.L., and Wang, P.X., 2001, Algal blooms: The primary mechanism in the formation of lacustrine petroleum source rocks: Geological Review, v. 47, p. 207–211 [in Chinese with English abstract].

Liu, Q., Zhang, L.Y., Shen, Z.M., Kong, X.X., and Li, Z., 2004, Evolution of lake-basin types and occurrence of hydrocarbon source rocks in Dongying Depression: Acta Petrolei Sinica, v. 25, p. 42–45 [in Chinese with English abstract].

Loucks, R.G., and Ruppel, S.C., 2007, Mississippian Barnett Shale: Lithofacies and depositional setting of a deep-water shale-gas succession in the Fort Worth Basin, Texas: American Association of Petroleum Geologists Bulletin, v. 91, p. 579–601, doi:10.1306/11020606059.

Lu, S.Q., Chen, G.J., Wu, K.Y., and Feng, D.Y., 2013, Tectonic feature and evolution mechanism of central anticline belt of Dongying Sag, Bohai Bay Basin: Petroleum Geology & Experiment, v. 35, p. 274–279 [in Chinese with English abstract].

Macquaker, J.H.S., and Adams, A.E., 2003, Maximizing information from fine-grained sedimentary rocks: An inclusive nomenclature for mudstones: Journal of Sedimentary Research, v. 73, p. 735–744, doi:10.1306/012203730735.

Macquaker, J.H.S., Taylor, K.G., and Gawthorpe, R.L., 2007, High-resolution facies analyses of mudstones: Implications for paleoenvironmental and sequence-stratigraphic interpretations of offshore ancient mud-dominated successions: Journal of Sedimentary Research, v. 77, p. 324–339, doi:10.2110/jsr.2007.029.

Macquaker, J.H.S., Bentley, S.J., and Bohacs, K.M., 2010a, Wave-enhanced sediment-gravity flows and mud dispersal across continental shelves: Reappraising sediment transport processes operating in ancient mudstone successions: Geology, v. 38, p. 947–950, doi:10.1130/G31093.1.

Macquaker, J.H.S., Keller, M.A., and Davies, S.J., 2010b, Algal blooms and "marine snow": Mechanisms that enhance preservation of organic carbon in ancient fine-grained sediments: Journal of Sedimentary Research, v. 80, p. 934–942, doi:10.2110/jsr.2010.085.

Milliken, K., 2014, A compositional classification for grain assemblages in fine-grained sediments and sedimentary rocks: Journal of Sedimentary Research, v. 84, p. 1185–1199, doi:10.2110/jsr.2014.92.

Ochoa, J., Wolak, J., and Gardner, M.H., 2013, Recognition criteria for distinguishing between hemipelagic and pelagic mudrocks in the characterization of deep-water reservoir heterogeneity: American Association of Petroleum Geologists Bulletin, v. 97, p. 1785–1803, doi:10.1306/04221312086.

Piper, D.Z., and Calvert, S.E., 2009, A marine biogeochemical perspective on black shale deposition: Earth-Science Reviews, v. 95, p. 63–96, doi:10.1016/j.earscirev.2009.03.001.

Plint, A.G., 2014, Mud dispersal across a Cretaceous prodelta: Storm-generated, wave-enhanced sediment gravity flows inferred from mudstone microtexture and microfacies: Sedimentology, v. 61, p. 609–647, doi:10.1111/sed.12068.

Potter, P.E., Maynard, J.B., and Depetris, P.J., 2005, Mud and Mudstones: New York, Springer, p. 137–142.

Qiu, N.S., Su, X.G., Li, Z.Y., Liu, Z.Q., and Li, Z., 2006, The Cenozoic tectono-thermal evolution of Jiyang Depression, Bohai Bay Basin, East China: Chinese Journal of Geophysics, v. 49, p. 1015–1024 [in Chinese with English abstract], doi:10.1002/cjg2.923.

Ren, J.Y., and Zhang, Q.L., 2004, Analysis of development mechanism for center uplift belt in Dongying Depression: Geotectonica et Metallogenia, v. 28, p. 254–262.

Roop, H.A., Dunbar, G.B., Levy, R., Vandergoes, M.J., Forrest, A.L., Walker, S.L., Purdie, J., Upton, P., and Whinney, J., 2015, Seasonal controls on sediment transport and deposition in Lake Ohau, South Island, New Zealand: Implications for a high-resolution Holocene palaeoclimate reconstruction: Sedimentology, v. 62, p. 826–844, doi:10.1111/sed.12162.

Schieber, J., 1999, Distribution and deposition of mudstone facies in the Upper Devonian Sonyea Group of New York: Journal of Sedimentary Research, v. 69, p. 909–925, doi:10.2110/jsr.69.909.

Schieber, J., and Southard, J.B., 2009, Bedload transport of mud by floccule ripples—Direct observation of ripple migration processes and their implications: Geology, v. 37, p. 483–486, doi:10.1130/G25319A.1.

Schieber, J., Southard, J., and Thaisen, K., 2007, Accretion of mudstone beds from migrating floccule ripples: Science, v. 318, p. 1760–1763, doi:10.1126/science.1147001.

Schieber, J., Southard, J.B., and Schimmelmann, A., 2010, Lenticular shale fabrics resulting from intermittent erosion of water-rich muds: Interpreting the rock record in the light of recent flume experiments: Journal of Sedimentary Research, v. 80, p. 119–128, doi:10.2110/jsr.2010.005.

Sheng, W.B., Cao, Y.C., Liu, H., and Zhang, Y., 2008, Evolutionary characteristics of the Palaeogene basin-controlling boundary faults and types of basin architectures in the Dongying Depression: Oil & Gas Geology, v. 29, p. 290–296 [in Chinese with English abstract].

Slatt, R.M., 2007, Introduction to the petroleum geology of deepwater setting, *in* Weimer, P., and Slatt, R.M., Introduction to the Petroleum Geology of Deepwater Setting: American Association of Petroleum Geologists Studies in Geology 57, p. 1–18.

Song, G.Q., Zhang, L.Y., Lu, S.F., Xu, X., Zhu, R., Wang, M., and Li, Z., 2013, Resource evaluation method for shale oil and its application: Earth Science Frontiers, v. 20, p. 221–228 [in Chinese with English abstract].

Soyinka, O.A. and Slatt, R.M., 2008, Identification and microstratigraphy of hyperpycnites and turbidites in Creta-

ceous Lewis Shale, Wyoming: Sedimentology, v. 55, p. 1117–1133, doi:10.1111/j.1365-3091.2007.00938.x.

Stow, D.A.V., and Bowen, A.J., 1980, Physical model for the transport and sorting of fine-grained sediment by turbidity currents: Sedimentology, v. 27, p. 31–46, doi:10.1111/j.1365-3091.1980.tb01156.x.

Stow, D.A.V., and Mayall, M., 2000, Deep-water sedimentary systems: New models for the 21st century: Marine and Petroleum Geology, v. 17, p. 125–135, doi:10.1016/S0264-8172(99)00064-1.

Stow, D.A.V., Huc, A.Y., and Bertrand, P., 2001, Depositional processes of black shales in deep water: Marine and Petroleum Geology, v. 18, p. 491–498, doi:10.1016/S0264-8172(01)00012-5.

Suo, Y.H., Li, S.Z., Dai, L.M., Liu, X., and Zhou, L.H., 2012, Cenozoic tectonic migration and basin evolution in East Asia and its continental margins: Acta Petrologica Sinica, v. 28, p. 2602–2618 [in Chinese with English abstract].

Tänavsuu-Milkeviciene, K., and Sarg, J.F., 2012, Evolution of an organic-rich lake basin-stratigraphy, climate and tectonics: Piceance Creek basin, Eocene Green River Formation: Sedimentology, v. 59, p. 1735–1768, doi:10.1111/j.1365-3091.2012.01324.x.

Thiry, M., 2000, Paleoclimatic interpretation of clay minerals in marine deposits: An outlook from the continental origin: Earth-Science Reviews, v. 49, p. 201–221, doi:10.1016/S0012-8252(99)00054-9.

Tian, J.C., Yin, G., Tan, J.X., Zeng, Y.F., and Li, Y.S., 1988, The relationship between the transgression of Eogene and the origin of lacustrine dolomitite in eastern China, taking the Shahejie Formation of Dongying Depression as example: China Offshore Oil and Gas (Geology), v. 12, p. 230–254 [in Chinese with English abstract].

Tindall, J., Flecker, R., Valdes, P., Schmidt, D.N., Markwick, P., and Harris, J., 2010, Modelling the oxygen isotope distribution of ancient seawater using a coupled ocean-atmosphere GCM: Implications for reconstructing early Eocene climate: Earth and Planetary Science Letters, v. 292, p. 265–273, doi:10.1016/j.epsl.2009.12.049.

Tucker, M.E., 2001, Sedimentary Petrology: New York, Wiley-Blackwell, p. 92–93.

Tyson, R.V., 2001, Sedimentation rate, dilution, preservation and total organic carbon: Some results of a modelling study: Organic Geochemistry, v. 32, p. 333–339, doi:10.1016/S0146-6380(00)00161-3.

Ver Straeten, C.A., Brett, C.E., and Sageman, B.B., 2011, Mudrock sequence stratigraphy: A multi-proxy (sedimentological, paleobiological and geochemical) approach, Devonian Appalachian Basin: Palaeogeography, Palaeoclimatology, Palaeoecology, v. 304, p. 54–73, doi:10.1016/j.palaeo.2010.10.010.

Wang, G.M., 2012, Laminae combination and genetic classification of Eogene shale in Jiyang Depression: Journal of Jilin University [Earth Science Edition], v. 42, p. 666–680.

Wang, J., Cao, Y.C., Liu, H.M., and Gao, Y.J., 2012, Characteristics of sedimentary environment and filling model of the Lower Submember of the Fourth Member of Shahejie Formation, Dongying Depression: Acta Sedimentologica Sinica, v. 30, p. 274–282 [in Chinese with English abstract].

Wang, Y.S., Li, Z., Gong, J.Q., Zhu, J.J., Hao, Y.Q., Hao, X.F., and Wang, Y., 2013, Discussion on an evaluation method of shale oil and gas in Jiyang depression: A case study on Luojia area in Zhanhua sag: Acta Petrolei Sinica, v. 34, p. 83–90 [in Chinese with English abstract].

Wu, J., Jiang, Z.X., Qian, K., and Xu, D., 2014, Characteristics of salinization mechanism on the upper part of fourth member of Shahejie Formation in the Dongying Depression, Shandong Province: Acta Geoscientica Sinica, v. 35, p. 733–740 [in Chinese with English abstract].

Wu, S.G., and Liu, W.C., 2004, Tectonics of subduction zone in the East Asia continental margin: Earth Science Frontiers, v. 11, p. 15–22 [in Chinese with English abstract].

Xu, J., Bechtel, A., Sachsenhofer, R.F., Liu, Z., Gratzer, R., Meng, Q., and Song, Y., 2015, High resolution geochemical analysis of organic matter accumulation in the Qingshankou Formation, Upper Cretaceous, Songliao Basin (NE China): International Journal of Coal Geology, v. 141–142, p. 23–32, doi:10.1016/j.coal.2015.03.003.

Xu, W., Chen, K.Y., Cao, Z.L., Xue, J.Q., Xiao, P., and Wang, W.T., 2014, Original mechanism of mixed sediments in the saline lacustrine basin: Yanshi Xuebao, v. 30, p. 1804–1816 [in Chinese with English abstract].

Xue, Y., Wu, Z.P., Li, W., and Nie, W.L., 2013, Cenozoic basin structure in the Dongying Depression and its control over reservoir: Geotectonica et Metallogenia, v. 37, p. 206–212 [in Chinese with English abstract].

Yang, H.Z., Ren, J., and Lu, J.B., 2009, Tectonic styles and kinematic characteristics of negative inversion structure in Dongying Depression: Earth Science-Journal of China University of Geosciences, v. 34, p. 493–501.

Yuan, J.Y., Huang, C.G., Cao, Z.L., Li, Z.Y., Wan, C.Z., Xu, L., Pan, X., and Wu, L.R., 2015, Carbon and oxygen isotopic composition of saline lacustrine dolomite and its palaeoenvironmental significance: A case study of Lower Eocene Ganchaigou Formation in western Qaidam Basin: Geochemica, v. 44, p. 254–266 [in Chinese with English abstract].

Yuan, W.F., Chen, S.Y., and Zeng, C.M., 2006, Study on marine transgression of Paleogene Shahejie Formation in Jiyang Depression: Acta Petrolei Sinica, v. 27, p. 40–49 [in Chinese with English abstract].

Zhang, P.Z., Zhang, H.P., Zheng, W.J., Zheng, D.W., Wang, W.T., and Zhang, Z.Q., 2014, Cenozoic tectonic evolution of continental eastern Asia: Seismology and Geology, v. 36, no. 3, p. 574–585.

Zhao, L., and Li, L., 2016, The extensional pattern and dynamics of Bohai Bay Basin in late Mesozoic–Cenozoic: Geology in China, v. 43, p. 470–485.

Zhu, G.Y., and Jin, Q., 2003, Geochemical characteristics of two sets of excellent source rocks in Dongying Depression: Acta Sedimentologica Sinica, v. 21, p. 506–512 [in Chinese with English abstract].

Zhu, G.Y., Jin, Q., Zhang, S.C., Dai, J.X., Wang, G.M., Zhang, L.Y., and Li, J., 2005, Characteristics and origin of deep lake oil shale of the Shahejie Formation of Paleogene in Dongying Depression: Journal of Palaeogeography, v. 7, p. 59–69 [in Chinese with English abstract].

Zou, C.N., Yang, Z., and Cui, J.W., 2013, Formation mechanism, geological characteristics and development strategy of nonmarine shale oil in China: Petroleum Exploration and Development, v. 40, p. 15–27, doi:10.1016/S1876-3804(13)60002-6.

Science Editor: David I. Schofield
Associate Editor: Wenjiao Xiao

Manuscript Received 25 May 2016
Revised Manuscript Received 24 April 2017
Manuscript Accepted 26 June 2017

Printed in the USA